AD-A173 215 EFFECTIVE FINITE ELEMENTS FOR SHELL ANALYSIS(U) 1/1
NORTHWESTERN UNIV EVANSTON IL DEPT OF CIVIL ENGINEERING
T BELYTSCHKO ET AL. 20 FEB 84 AFOSR-TR-86-0891
UNCLASSIFIED F49620-82-K-0013 F/G 13/13 NL

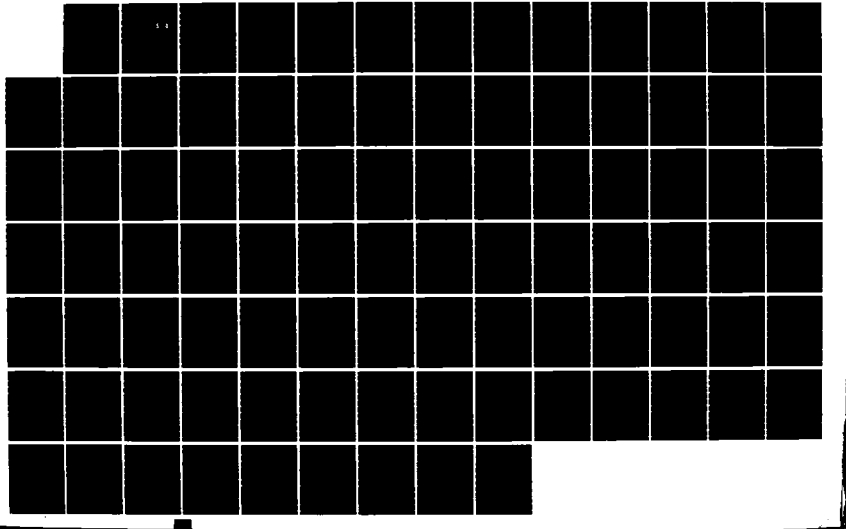

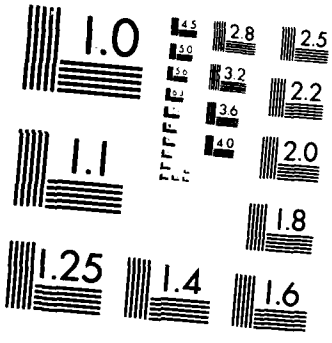

(2)

AFOSR-TR- 86-0891

EFFECTIVE FINITE ELEMENTS FOR SHELL ANALYSIS

by

T. Belytschko
H. Stolarski
W.K. Liu
and
N. Carpenter

UNCLASSIFIED

SECURITY CLASSIFICATION OF THIS PAGE

REPORT DOCUMENTATION PAGE

1a. REPORT SECURITY CLASSIFICATION	1b. RESTRICTIVE MARKINGS
2a. SECURITY CLASSIFICATION AUTHORITY UNCLASSIFIED	3. DISTRIBUTION/AVAILABILITY OF REPORT Approved for public release; distribution unlimited
2b. DECLASSIFICATION/DOWNGRADING SCHEDULE	
4. PERFORMING ORGANIZATION REPORT NUMBER(S)	5. MONITORING ORGANIZATION REPORT NUMBER(S) **AFOSR-TR- 86-0891**
6a. NAME OF PERFORMING ORGANIZATION Northwestern University 6b. OFFICE SYMBOL (If applicable)	7a. NAME OF MONITORING ORGANIZATION AFOSR
6c. ADDRESS (City, State and ZIP Code) Department of Civil Engineering Evanston, Illinois 60201	7b. ADDRESS (City, State and ZIP Code) Bolling AFB DC 20332-6448
8a. NAME OF FUNDING/SPONSORING ORGANIZATION Air Force Office of Scientific Research 8b. OFFICE SYMBOL (If applicable) AFOSR/NA	9. PROCUREMENT INSTRUMENT IDENTIFICATION NUMBER<br~~F49620-~~ ~~AFOSR-~~82-K-0013
8c. ADDRESS (City, State and ZIP Code) Bolling AFB, DC 20332- 6448	10. SOURCE OF FUNDING NOS. PROGRAM ELEMENT NO. 61102F; PROJECT NO. 2302 ~~2307~~; TASK NO. B1 ~~G2~~; WORK UNIT NO.
11. TITLE (Include Security Classification) Effective Finite Elements for Shell Analysis (UNCLASSIFIED)	
12. PERSONAL AUTHOR(S) T. Belytschko, H. Stolarski, W.K. Liu, N. Carpenter	
13a. TYPE OF REPORT Final 13b. TIME COVERED FROM Feb.1,83 TO Jan30,84	14. DATE OF REPORT (Yr., Mo., Day) Feb 20, 1984 15. PAGE COUNT
16. SUPPLEMENTARY NOTATION	

17. COSATI CODES			18. SUBJECT TERMS (Continue on reverse if necessary and identify by block number)
FIELD	GROUP	SUB. GR.	
			Structures, Finite Element, Shells, Locking, Spurious Modes

19. ABSTRACT (Continue on reverse if necessary and identify by block number)

One of the major difficulties in the formulation of effective shell elements has been identified to be the phenomenon of membrane locking. Membrane locking occurs in curved shell elements when the in-plane displacement approximation is not of higher order than the transverse displacement approximation and inextensional bending of the shell cannot take place. Inextensional bending is an important mode of deformation, and when an element is not capable of representing inextensional bending, parasitic membrane energy is generated in many modes of deformation. In the same manner that parasitic shear causes shear locking, this spurious membrane energy causes membrane locking. Membrane locking severely reduces the rate of convergence of shell elements, particularly in deep shells and in situations where the bending of the shell is the dominant mode of deformation.

(cont.)

20. DISTRIBUTION/AVAILABILITY OF ABSTRACT UNCLASSIFIED/UNLIMITED ☒ SAME AS RPT. ☐ DTIC USERS ☐	21. ABSTRACT SECURITY CLASSIFICATION UNCLASSIFIED
22a. NAME OF RESPONSIBLE INDIVIDUAL Dr. Anthony Amos	22b TELEPHONE NUMBER (Include Area Code) (202)767-4937 22c. OFFICE SYMBOL AFOSR/NA

DD FORM 1473, 83 APR EDITION OF 1 JAN 73 IS OBSOLETE

UNCLASSIFIED

SECURITY CLASSIFICATION OF THIS PAGE

19. ABSTRACT (cont.)

In this report, two methods for eliminating membrane locking in curved shell elements are presented. The first method is a strain projection method in which the membrane strains are corrected so that inextensional modes of pure bending become possible. The method is applied both to a curved beam element and a traingular shell element in which the flexural behavior is modeled by a discrete Kirchhoff theory. The use of this projection method introduces membrane-flexural coupling to the shell element and modifies the bending stiffness in an appropriate fashion. Results have been obtained with this element for linear analysis of static response of deep shell structures and for nonlinear, collapse analysis of columns and cylindrical panels. The results show a remarkably rapid rate of convergence.

The second method which is under investigation for avoiding membrane locking is the use of uniform reduced quadrature on the 9-node Lagrange element. Results obtained in the previous study by the author suggests that if 2 x 2 quadrature could be used in the curved shell element, membrane locking as well as shear locking could be avoided, and thus very rapid rates of convergence would be achieved. However, the use of uniform reduced quadrature is accompanied by the appearance of spurious zero energy modes which can yield meaningless answers to solutions for certain boundary conditions.

In this investigation, a spurious mode control scheme has been developed for the 9-node plate which eliminates spurios modes completely. The method is based on retaining the formal consistency of the governing equations of the systems, which is equivalent to satisfying the patch test. As a result of these properties of the spurious mode control method, results which have been obtained for this plate show nearly the optimal h^3 of convergence.

TABLE OF CONTENTS

INTRODUCTION

One of the major difficulties in the formulation of effective shell elements has been identified to be the phenomenon of membrane locking. Membrane locking occurs in curved shell elements when the in-plane displacement approximation is not of higher order than the transverse displacement approximation and inextensional bending of the shell cannot take place. Inextentional bending is an important mode of deformation, and when an element is not capable of representing inextensional bending, parasitic membrane energy is generated in many modes of deformation. In the same manner that parasitic shear causes shear locking, this spurious membrane energy causes membrane locking. Membrane locking severely reduces the rate of convergence of shell elements, particularly in deep shells and in situations where the bending of the shell is the dominant mode of deformation.

In this report, two methods for eliminating membrane locking in curved shell elements are presented. The first method is a strain projection method in which the membrane strains are corrected so that inextensional modes of pure bending become possible. The method is applied both to a curved beam element and a triangular shell element in which the flexural behavior is modeled by a discrete Kirchhoff theory. The use of this projection method introduces membrane-flexural coupling to the shell element and modifies the bending stiffness in an appropriate fashion. Results have been obtained with this element for linear analysis of static response of deep shell structures and for nonlinear, collapse analysis of columns and cylindrical panels. The results show a remarkably rapid rate of convergence.

The second method which is under investigation for avoiding membrane locking is the use of uniform reduced quadrature on the 9-node Lagrange

element. Results obtained in the previous study by the author suggests that if 2 x 2 quadrature could be used in the curved shell element, membrane locking as well as shear locking could be avoided, and thus very rapid rates of convergence would be achieved. However, the use of uniform reduced quadrature is accompanied by the appearance of spurious zero energy modes which can yield meaningless answers to solutions for certain boundary conditions.

In this investigation, a spurious mode control scheme has been developed for the 9-node plate which eliminates spurious modes completely. The method is based on retaining the formal consistency of the governing equations of the systems, which is equivalent to satisfying the patch test. As a result of these properties of the spurious mode control method, results which have been obtained for this plate show nearly the optimal h^3 of convergence.

In Chapter 1 of this report, the projection methods are developed. In the first section, the projection method is developed for a curved beam in order to illustrate its essential features. Section 2 then uses the developments for curved beams in a very simple fashion to develop a projection operator for the 3-node triangular plate element; this element uses a constant state of membrane strain and either the discrete Kirchhoff theory DKT flexural element or a C^0 bending formulation with one quadrature point. Results are then given in Section 3 for a series of static problems and two dynamic problems involving the collapse of shell structures.

In Chapter 2, the procedure for spurious zero energy mode control for the 9-node element is developed. The development is first given in the setting of the Laplace equation, where the role of the spurious mode control procedure is quite transparent and the important role of maintaining consistency with the

spurious mode control procedure is illustrated. Results obtained for the Laplace equation show that by using the spurious mode control procedure, convergence in the L_2 norm of order h^3 can be achieved for rectangular meshes, whereas some deterioration in the rate of convergence results when the elements are curved or skewed. However, the same deterioration in the rate of convergence occurs if selective reduced integration is used. The method is then applied to plate problems. A large series of plate problems, some of them involving situations where convergence is very slow, such as a rhombic plate modeled by parallelogram elements are considered. In all cases, very rapid rates of convergence are achieved with this element and no spurious modes are present.

CHAPTER 1

STRAIN PROJECTION METHODS FOR CONSTANT STRAIN ELEMENTS

1. Introduction

The development of an effective but simple shell element which incorporates the effects of the curvature of the shell but avoids locking and spurious kinematic modes is essential for effective and economical analysis of shells in the failure domain. However, while elements such as the 16 node C^0 element are quite accurate, their complexity and high cost makes them unattractive for nonlinear analysis. Lower order or flat elements, on the other hand, tend to be excessively stiff and a very large number are required for accuracy.

In this paper we sketch the development of a simple, curved, triangular-shell element. The element has the following advantages:

1. It correctly represents rigid body motion.
2. It correctly represents states of constant membrane strains and constant curvatures, and thus allows for inextensional bending and eliminates membrane locking [1].
3. It couples bending and membrane effects within an element.
4. As opposed to various elements based on selective reduced integration, it possesses no kinematic modes [2-4].
5. While it is perhaps the simplest curved shell element (compare [5-17]) the element yields surprisingly accurate results, often superior to those obtained by more complex elements.

The basis for this element is the mode decomposition technique described for the curved beam in [18] in conjunction with a shallow shell theory. It

should be noted that contrary to the results of earlier investigators [12,19], use of a shallow shell theory in our case does not diminish the element's performance in deep shell problems.

The mode decomposition technique is used to achieve an element free of membrane locking and with the correct relationship between membrane and bending effects. The DKT (discrete Kirchhoff theory) element [20,21] (see also [22-24]) is used to form the bending part of the stiffness matrix. This portion of the stiffness matrix may be replaced with any other triangular plate-element stiffness matrix provided that corners are the only nodal points of the element. However, the most rigorous justification of the development presented herein is related to the DKT element.

To make the paper self-contained, we begin with a short presentation of the major ideas in the context of curved beams. This is followed by a development of the triangular shell element. Finally, the performance of this element is demonstrated by a number of solutions to various shell problems. Some general remarks conclude the paper.

2. Curved Beam Element

A conclusion that can be drawn from [25-32] is that the ability to represent independent bending and membrane strain states is crucial for the success of a curved beam or shell element. However, satisfaction of this requirement is difficult and has only been accomplished by using the so-called assumed strain elements [26,27,30]. Unfortunately, this approach appears impossible for arbitrary shell elements and so far only cylindrical shell elements have been formulated by this method [33-35]. Another important conclusion of past research is that the proper inclusion of rigid body motion

considerably improves element's performance [36-39], but this is not central to the topic of this paper.

In [18] (see also [40]) a different approach has been taken to meeting these conditions. It allows for simultaneous existence of both membrane and bending strains in all patterns of deformations but, at the same time, for any given set of nodal degrees of freedom, it defines certain modes of deformation from which the membrane strain energy is removed. Since only the bending strain energy is assigned to these modes, we call them bending modes. The remaining portion of the total deformation is called the membrane mode. This modification of the membrane strain energy results in a modified and better element stiffness. A theoretical justification for this approach to curved beams through the Hu-Washizu variational principle is given in [18].

To describe how the bending mode and consequently the membrane mode is defined, consider the curved beam shown in Fig. 1. To properly account for rigid body motion and for the sake of simplicity, we consider the element in a corotating frame whose x-axis passes through both of its ends. A theory of shallow structures will be used with the following kinematical relationships

$$\varepsilon = u_{,x} + w^{o}_{,x}\, w_{,x} \tag{1a}$$

$$\kappa = - w_{,xx} \tag{1b}$$

where w^{o} describes the initial shape of the element, u and w are displacements, parallel and perpendicular to the chord respectively. The deformational degrees of freedom are

$$\underset{\sim}{d}^T = [u_{21}, \phi_1, \phi_2], \qquad u_{21} = u_2 - u_1 \tag{2a}$$

$$\phi_1 = \phi_1^{tot} - \frac{1}{L}(w_2 - w_1) \tag{2b}$$

$$\phi_2 = \phi_2^{tot} - \frac{1}{L}(w_2 - w_1) \tag{2c}$$

where u_{21} is the relative longitudal displacement of the right end with respect to the left one, ϕ_I are the deformational rotations and ϕ_I^{tot} the total rotations of the nodes.

The following interpolations are used for u, w and w^o.

$$u = u_{21}\,\xi \tag{3a}$$

$$w = L\,(\phi_1 N_1 + \phi_2 N_2) \tag{3b}$$

$$w^o = L\,(\alpha_1 N_1 + \alpha_2 N_2) \tag{3c}$$

where α_1, α_2 are rotations associated with the initial shape of the element, L is its lenyth and

$$N_1 = \xi - 2\xi^2 + \xi^3 \tag{4a}$$

$$N_2 = \xi^3 - \xi^2 \tag{4b}$$

$$\xi = \frac{x}{L} \tag{4c}$$

In view of Eq. (1b) it is evident that the distribution of curvatures is related exclusively to w. However, based on Eqs. (3a,3b) and (1a) it is also evident that for any $\kappa \neq 0$, when $w_0 \neq 0$ then $\varepsilon \neq 0$, so inextensible bending states are impossible for the approximation given in Eq. (3). This is precisely the cause of membrane locking discussed in [1]. However, as opposed to the reduced integration employed in [2], membrane locking can be eliminated by mode decomposition [18], which provides a more rational and accurate method.

In the decomposition technique, through physical arguments certain modes of deformation are required to be free of membrane strain energy. An operator is then developed so that the element satisfies these requirements. For example, in a curved beam, the nodal displacements are decomposed into bending and membrane modes. In bending modes, the membrane strain energy is required to vanish. A similar approach has been developed to avoid shear locking [3].

To define the bending mode of this decomposition, note that in inextensional bending, the chord of a curved beam must, in general, change in the length. This longitudinal displacement u_{21}^b is associated with the rotations ϕ_1 and ϕ_2 and define the bending mode. This mode of deformation must be free of membrane strain energy for inextensional bending to be possible, which is imperative if membrane locking is to be avoided.

The bending mode can be easily determined by considering that, for the displacement fields given in Eq. (3b,3c), and the curvature field defined in Eq. (1b), inextensional bending is accompanied by the following extension of the chord

$$u_{21}^{b} = -\int_{0}^{L} w_{,x}^{o}\, w_{,x}\, dx = \phi_1 L \left(-\frac{2}{15}\alpha_1 + \frac{1}{30}\alpha_2\right) + \phi_2 L \left(-\frac{2}{15}\alpha_2 + \frac{1}{30}\alpha_1\right) \tag{5}$$

If it is assumed that $\varepsilon = 0$ (inextensibility) the expression can be derived from Eq. (1a). The complete set of nodal degrees of freedom in the bending mode is therefore

$$(\underset{\sim}{d}^{b})^{T} = [u_{21}^{b},\ \phi_1,\ \phi_2] \tag{6}$$

Since the sum of the two deformation modes gives the total deformation, the membrane mode is described by

$$(\underset{\sim}{d}^{m})^{T} = [u_{21} - u_{21}^{b},\ 0,\ 0] \tag{7}$$

The strains related to both of the above modes can be computed according to Eqs. (1a,1b). However, the membrane strain energy associated with the membrane mode should only be considered in deriving the stiffness. Thus the strain energy is given by

$$U = \frac{1}{2}\int_{0}^{L} D_b\, \kappa^2\, dx + \frac{1}{2}\int D_m\, \bar{\varepsilon}^2\, dx \tag{8}$$

where

$$D_b = EI, \qquad D_m = EA , \qquad \bar{\varepsilon} = \frac{u_{21} - u_{21}^b}{L} \tag{9}$$

and E is Young modulus, I the moment of inertia and A the cross-sectional area. The element stiffness matrix, as usual, is obtained from Eq. (8) and is given in terms of the deformational degrees of freedom $\underset{\sim}{d}$ by

$$\hat{\underset{\sim}{K}} = \frac{EI}{L} \begin{bmatrix} \frac{R}{L^2} & \frac{Rc_1}{L} & \frac{Rc_2}{L} \\ \frac{Rc_1}{L} & 4 + Rc_1^2 & 2 + Rc_1c_2 \\ \frac{Rc_2}{L} & 2 + Rc_1c_2 & 4 + Rc_2^2 \end{bmatrix} \tag{10a}$$

where

$$R = \frac{AL^2}{I} \tag{10b}$$

$$c_1 = \frac{2}{15}\alpha_1 - \frac{1}{30}\alpha_2 \tag{10c}$$

$$c_2 = \frac{2}{15}\alpha_2 - \frac{1}{30}\alpha_1 \tag{10d}$$

The global stiffness matrix is

$$\underset{\sim}{K} = \underset{\sim}{T}_1^T \hat{\underset{\sim}{K}} \underset{\sim}{T}_1 \tag{11}$$

$$\underset{\sim}{T}_1 = \begin{bmatrix} -c & -s & 0 & c & s & 0 \\ s/L & -c/L & 1 & -s/L & c/L & 0 \\ s/L & -c/L & 0 & -s/L & c/L & 1 \end{bmatrix} \qquad (12a)$$

$$s = (y_2 - y_1)/L \qquad c = (x_2 - x_1)/L \qquad (12b)$$

It is important to note that inextensional bending is now possible and that, through the nonzero values of $\hat{K}_{12}$ and $\hat{K}_{13}$, coupling between membrane and flexural behavior is introduced. Hence the main characteristic of a curved element is retained.

Remarks:

1. Although a physical approach has been presented here, a formal equivalence between the above formulation and a mixed formulation has been established in [18]; the technique can also be viewed as a strain projection method.
2. It can be shown that this formulation is also equivalent to an "exact" (without any modifications or reduced integration) displacement formulation which can be obtained from the present one by replacing the linear interpolation for u given in Eq. (3a) by a fifth-order polynomial that satisfies $\varepsilon = 0$ at each point of the beam.
3. The same approach can also be adopted for higher order elements, [18]. However, the higher the order of the element, the less severe the membrane locking [2].

4. For a straight beam, the stiffness matrix obtained from Eq. (8) reduces to two matrices: a bar matrix and a beam matrix with no interaction between them.

3. Curved Triangular Shell Element

The triangular shell element has three nodes at its corners and the corotational plane (x, y) is always defined by these nodes as shown in Fig. 2. The vectors $\underset{\sim}{e}_I$, I = 1 to 3, are unit vectors in the positive directions of the local coordinates of the sides, $\xi_I \in (0,1)$.

The nodal degrees of freedom at each node are

$$\underset{\sim}{d}_I^{tot} = (u_{xI}^{tot}, u_{yI}^{tot}, w_I^{tot}, \theta_{xI}^{tot}, \theta_{yI}^{tot}) \qquad I = 1 \text{ to } 3 \tag{13}$$

For simplicity, the basic developments will be presented in terms of deformation nodal displacements

$$\underset{\sim}{d}^T = (\underset{\sim}{n}^T, \underset{\sim}{\theta}^T) \tag{14a}$$

$$\underset{\sim}{n}^T = (n_1, n_2, n_3) \tag{14b}$$

$$\underset{\sim}{\theta}^T = (\theta_{x1}, \theta_{y1}, \theta_{x2}, \theta_{y2}, \theta_{x3}, \theta_{y3}) \tag{14c}$$

where n_I is the elongation of side I and θ_{xI}, θ_{yI} are the deformation nodal rotations at the node I, which are given by

$$\theta_{xI} = \theta_{xI}^{tot} - \omega_x \tag{15a}$$

$$\theta_{yI} = \theta_{yI}^{tot} - \omega_y \tag{15b}$$

where ω_x and ω_y are the rigid body rotations of the element.

The membrane state of strain is considered constant with linear u_x and u_y and the discrete Kirchhoff theory (DKT) is used to describe the bending properties of the element. In the DKT element, the rotation field is quadratic and the transverse displacements are cubic along each of the sides [20].

It should be noted that the discrete Kirchhoff constraints are imposed at three points along each side, which guarantees orthogonality of the tangential component of the normals to the midline at any point of the side (see [20,21] for details). Therefore each side of the element deforms in exactly the same fashion as the curved beam based on Kirchhoff (not discrete Kirchhoff) theory, described in the previous section. Thus, if the in-plane displacements are linear (strains are constant), inextensional bending is not possible.

Therefore, a modification similar to that employed in the curved beam element is made: the in-plane elongations which should accompany inextensional bending are first determined, and their contributions to the membrane strain energy then are removed.

The initial curved shape of the element is described by $w^o(x, y)$, which along each of the sides I is given by

$$w^o(\xi_I) = \alpha_1^I \ell_I N_1(\xi_I) + \alpha_2^I \ell_I N_2(\xi_I) \tag{16}$$

where α_1^I and α_2^I are the initial rotations of the midline for side I, ℓ_I the length of side I, and $N_J(\xi)$ are given by Eqs. (4).

In the DKT element, the transverse displacements along each side are given by

$$w(\xi_I) = \phi_1^I \ell_I N_1(\xi_I) + \phi_2^I \ell_I N_2(\xi_I) \tag{17}$$

where

$$\phi_1^I = \theta_{xJ} e_{Iy} - \theta_{yJ} e_{Ix} \tag{18a}$$

$$\phi_2^I = \theta_{xI} e_{Iy} - \theta_{yI} e_{Ix} \tag{18b}$$

and $J = I - 1$, $J = 3$ for $I - 1 = 0$.

The elongational strain and curvature along each edge are given by

$$\epsilon_s = u_{s,s} + w_{,s}^o w_{,s} \tag{19a}$$

$$\kappa_s = - w_{,ss} \tag{19b}$$

From the similarity of Eqs. (1) and (3) to (16), (17) and (19), it is readily apparent that each side of the plate behaves exactly like the curved beam described in the previous section. Thus, if inextensional bending of the shell element is to be possible, the elongations of the chords associated with bending must be omitted from the membrane strain energy.

The bending elongation component of each side is given by the counterpart

of Eq. (5),

$$\eta_I^b = \frac{1}{30}\,\phi_1^I\,\ell_I\,(-4\alpha_1^I + \alpha_2^I) + \frac{1}{30}\,\phi_2^I\,\ell_I\,(\alpha_1^I - 4\alpha_2^I) \tag{20}$$

Thus if the total strain energy is taken to be

$$U = \frac{1}{2}\,\underset{\sim}{\theta}^T\,\underset{\sim}{K}_b\,\underset{\sim}{\theta} + \frac{1}{2}\,(\underset{\sim}{\eta} - \underset{\sim}{\eta}^b)\,\underset{\sim}{K}_m\,(\underset{\sim}{\eta} - \underset{\sim}{\eta}^b) \tag{21}$$

then bending without any membrane strain energy will always be possible. In the above, $\underset{\sim}{K}_b$ is the plate bending stiffness of the element expressed in terms of its 6 deformation modes, $\underset{\sim}{\theta}$, and $\underset{\sim}{K}_m$ the membrane stiffness expressed in terms of the deformation modes $\underset{\sim}{\eta}$; $\underset{\sim}{K}_m$ is identical to the stiffness of the well-known constant-strain triangle but expressed in an alternate set of degrees of freedom, it is given in Appendix A. It is also possible to describe $\underset{\sim}{K}_m$ directly in terms of nodal displacements.

It is convenient to express $\underset{\sim}{\eta}^b$ in terms of $\underset{\sim}{\theta}$ by

$$\underset{\sim}{\eta}^b = \underset{\sim}{I}\,\underset{\sim}{\theta} \tag{22}$$

where $\underset{\sim}{I}$ is given in Appendix A. Using Eq. (21-22), the stiffness of the shell element can be shown to be given in terms of the deformation degrees of freedom by

$$\underset{\sim}{K} = \begin{bmatrix} \underset{\sim}{K}_m & -\underset{\sim}{K}_m\,\underset{\sim}{I} \\ -\underset{\sim}{I}^T\,\underset{\sim}{K}_m & \underset{\sim}{K}_b + \underset{\sim}{I}^T\,\underset{\sim}{K}_m\,\underset{\sim}{I} \end{bmatrix} \tag{23}$$

In the above equation, the effect of the decomposition becomes transparent:

1) it introduces membrane-flexural coupling through the terms $\underset{\sim}{K}_{m}\underset{\sim}{T}$.

2) it allows the membrane stiffness to effect the bending stiffness.

These effects are absent in any flat shell element. Thus, the most important features of a curved element are embodied in this element.

Remarks:

1. In this element, independent states of arbitrary curvatures (bending modes) and membrane strains (membrane modes) are possible. Thus the element can always bend without extension. Although not all shells allow for inextensional bending (see [32] for example), the ability of the element to undergo inextensional bending, regardless of its shape, is beneficial, because if inextensional bending is not possible in a particular shell, the appropriate restrictions on the bending are introduced by interactions between elements, but not the element itself.
2. For linear problems, the element stiffness matrix of Eq. (23) can be expressed in closed form, so no numerical integration is needed. This results from the fact that all the matrices involved in Eq. (23) can be expressed in a closed form (see [21] and [41] for details).
3. For a plate problem $\underset{\sim}{I} = \underset{\sim}{Q}$ and no interaction between bending and membrane effects exists.
4. Equation (20) is fundamental in deriving the element stiffness matrix for the curved triangular shell element. It is valid for a cubic approximation for the initial shape of the element sides and a cubic approximation of transverse displacements. For those reasons, the DKT element which incorporates cubic transverse displacements along each of its sides seems to be appropriate for the present development. However, other ele-

ments can be formulated with cubic interpolations along each side. The matrix $\underset{\sim}{T}$ of Eq. (22) would then remain the same but the matrix $\underset{\sim}{K}_b$ of Eq. (23) may change. Therefore $\underset{\sim}{K}_b$ can be associated with other formulations of the triangular plate element without changing the matrix $\underset{\sim}{T}$. In addition to the results obtained with $\underset{\sim}{K}_b$ associated with the DKT element, results obtained with $\underset{\sim}{K}_b$ from an earlier paper [4] will be presented (see also [3]). This matrix was found to closely approximate that of the DKT element although it is simpler and more economical computationally.

4. Numerical Results

Results are presented for a variety of linear static and nonlinear transient problems. The purpose of the first set of examples is to illustrate the enhanced accuracy of the curved element over a flat element, and to verify the absence of membrane locking. Moreover, some deep shell problems are considered to emphasize that elements based on shallow theory do converge to the deep shell solution. The second set of problems serves simply to illustrate the potential of this element in highly nonlinear situations such as encountered in collapse and post-buckling analysis.

Results are presented for two bending stiffnesses: the DKT stiffness [21] and the C^0 bending stiffness developed in [3,4].

Bending of an Infinite Circular Cylindrical Shell

The problem description is given in Fig. 3. This is in fact an arch in a state of plane strain. The problem has been solved with the curved shell element and with a flat element. The results normalized with respect to the analytic solution are given in Table 1. As can be seen, the results improve

dramatically when the initial curvature is taken into account.

For a different arrangement of elements, the results obtained with the flat elements may be better. However, in the analysis of general shells, the selection of a mesh is not as easy as in this case. We therefore have selected the mesh shown in Fig. 3 to illustrate that a combination of flat elements and an inappropriate mesh can result in a considerable stiffening of the model. Our element successfully avoids this problem.

Pinched Cylinder with Free Edges

The cylinder and the related data are given in Fig. 4. This problem has been analyzed by many authors and their results are compared to ours in Tables 2 and 3. The total number of degrees of freedom was the same for all solutions. Both curved and flat elements with both the DKT and the C^0 bending formulations were used. It is clear that our element compares very well with the most accurate elements of others, including formulations which were designed specifically for cylindrical shells, [36], [43].

It is interesting to see that in this case the improvement achieved with curved elements is small. This is perhaps because the variation of displacements along the meridian of the shell is relatively small (in spite of the concentrated force) due to the small ratio of length to radius (see Fig. 4). This problem is not a demanding test on the performance of curved shell elements.

Pinched Cylinder with Diaphragms

The problem and pertinent data is depicted on Fig. 5. The results obtained with both curved and flat DKT elements along with those presented in [42] are reported in Table 4. The erratic behavior for the 2 x 2 mesh is due

to the inadequacy of the shallow shell theory for the relatively deep element emerging from such a coarse mesh. A considerable improvement is obtained with curved elements.

Impulsively Loaded Cylindrical Panel

This problem is defined in Fig. 6 and Table 5. The ends of the panel are simply-supported, while the side boundaries are fixed. Both material and geometric nonlinearities were considered. The load was applied by prescribing the initial velocity given in Fig. 6 to the nodes in the region loaded by the explosive. Figure 7 shows an undeformed and deformed mesh. Table 5 compares the results obtained for various meshes to an experimental result. It can be seen that the convergence to the experimental value is relatively slow. The reason for this however, is not the accuracy of the element, but the extreme localization of deformation which occurs due to the formation of plastic hinges.

Collapse of a Hollow Column

Figure 8 shows the simulation of a hollow column loaded axially. The time history of the load and material and geometric properties may be found in Fig. 3 and Table 1 of Ref. [44], respectively, where results obtained with a 4 node quadrilateral element using one-point quadrature and hourglass control are also given. The results obtained with this element compare well with those obtained for the quadrilateral, except the model is somewhat stiffer. Note the severe change in cross-section which accompanies buckling.

References

1. H. Stolarski and T. Belytschko, "Membrane Locking and Reduced Integration for Curved Elements," Journal of Applied Mechanics, 49, 172-176, (1982).

2. H. Stolarski and T. Belytschko, "Shear and Membrane Locking in Curved C^0 Elements,"to appear in Comp. Meth. Appl. Mech. Eng.

3. T. Belytschko, H. Stolarski and N. Carpenter, "A C^0 Triangular Plate Element with One-Point Quadrature," to appear in Int. J. Num. Meth. Eng.

4. N. Carpenter, T. Belytschko and H. Stolarski, "Locking and Shear Scaling Factors in C^0 Bending Elements," to appear in Computers and Structures.

5. S. Utku, "Stiffness Matrices for Thin Triangular Elements of Nonzero Gaussian Curvature," AIAA Journal, 5, 1659-1667, (1967).

6. J.H. Argyris and D.W. Sharpf, "The SHEBA Family of Shell Elements for the Matrix Displacement Method," Aero. J., 72, 873-883, (1968).

7. G.E. Strickland and W.A. Loden, "A Doubly Curved Triangular Shell Element," Proc. of the Second Conference on Matrix Methods in Structural Mechanics, Wright-Patterson Air Force Base, Ohio, October 1968.

8. G. Bonnes, G. Dhatt, Y.M. Giroux and L.P.A. Robichaud, "Curved Triangular Elements for the Analysis of Shells," Proc. of the Second Conferences on Matrix Methods in Structural Mechanics, Wright-Peterson Air Force Base, Ohio, October 1968.

9. G.R. Cowper, E. Kosco, G. Lindberg and M. Olson, "Static and Dynamic Application of a High Precision Triangular Plate Bending Element," AIAA Journal, 7, 1957-1965, (1969).

10. G.R. Cowper, G.M. Lindberg and M.D. Olson,"A Shallow Shell Finite Element of Triangular Shape," Int. J. Solids Struct., 6, 1133-1156, (1970).

11. C. Brebbia and J.M. Deb Nath, "A Comparison of Recent Shallow Shell Finite Element Analysis, Int. J. Mech .Sci., 12(10), 849-857, (1970).

12. G.R. Cowper, G.M. Lindberg and M.D. Olson, "Comparison of Two High Precision Triangular Finite Elements for Arbitrary Deep Shells," Proc. of the Third Conference on Matrix Methods in Structural Mechanics, AFLC-WPAFB-Oct. 71 550, Wright Patterson Air Force Base, Ohio, October 1971.

13. G.M. Lindberg and M.D. Olson, "A High Precision Triangular Cylindrical Shell Finite Element," AIAA Journal, 9(3), 530-532 (1971).

14. D.J. Dawe, "High Order Triangular Finite Element for Shell Analysis," Int. J. Solids Struct., 11, 1097-1110, (1975).

15. R.H. Gallagher and G.R. Thomas, "A Triangular Element Based on Generalized Potential Energy Concepts", in Finite Elements for Thin Shells and Curved Members, D.G. Ashwell and R.H. Gallagher, (Eds.) pp. 155-169, Wiley, London, 1976.

16. G.A. Mohr, "Numerically Integrated Triangular Element for Doubly Curved Thin Shells,s" Comp. and Structures, 11(6), 565-572, (1980).

17. D. Karamanlidis, "A New Mixed Hybrid Finite Element Model for Static and Dynamic Analysis of Thin Plates in Bending," in Recent Advances in Engineering Mechanics and Their Impact on Civil Engineering Practice," W.F. Chen and A.D.M. Lewis (Eds.) Published by ASCE, 1983.

18. H. Stolarski, T. Belytschko and B.L. Wong, "Mode Decomposition in the Analysis of Arches and Shells of Revolution," to appear in Computers and Structures.

19. R.H. Gallagher, "Shell Elements," Proceedings of the 1st Conference on Finite Element Methods in Structural Mechanics, Bournemouth, 1, 1975.

20. J.L. Batoz, K.J. Bathe and L.W. Ho, "A Study of Three Node Triangular Plate Bending Elements," Int. J. Num. Meth. Eng., 15, 1771-1812, (1980).

21. J.L. Batoz, "An Explicit Formulation for an Efficient Triangular Plate-Bending Element," Int. J. Num. Meth. Eng., 18, 1077-1089, (1982).

22. G.A. Wempner, J.T. Oden and D.A. Kross, "Finite Element Analysis of Thin Shells," Proc. ASCE, EM6, 94, 1273-1294 (1968).

23. G. Dhatt, "An Efficient Triangular Shell Element," AIAA Journal, 8, 2100-2102 (1970).

24. J.L. Batoz, A. Chattopadhyay and G. Dhatt, "Finite Element Large Deflection Analysis of Shallow Shells," Int. J. Num. Meth. Eng., 10, 39-58 (1976).

25. A.B. Sabir and D.G. Ashwell, "A Stiffness Matrix for Shallow Shell Finite Elements," Int. J. Mech. Sci., 11(3), 269-279 (1969).

26. D.G. Ashwell, A.B. Sabir and T.M. Roberts, "Further Studies in the Application of Curved FInite Elements to Circular Arches," Int. J. Mech. Sci., 13, 507-517 (1971).

27. D.G. Ashwell, "The Behavior with Diminishing Curvature of Strain Based Arch Finite Elements," J. Sound Vib., 28, 133 (1973).

28. I Fried, "Basic Computational Aspects of the Finite Element Analysis of Shells," Int. J. Solids Struct., 7, 1705-1715 (1971).

29. I. Fried, "Shape Functions and the Accuracy of Arch Finite Elements," AIAA J., 11, 287 (1973).

30. D.G. Ashwell, "Strain Elements, with Applications to Arches, Rings and Cylindrical Shells," Finite Elements for Thin Shells and Curved Members, D.G. Ashwell and R.H. Gallagher (Eds.), John Wiley and Sons, 1976.

31. L.S.D. Morley, "Quality of Trial Functions in Quadratic Isoparametric Representation of an Arc," Int. J. Num. Meth. Eng. 19(1), 37-38 (1983).

32. L.S.D. Morley, "Approximation to Bending Trial Functions for Shell Triangular Finite Elements in Quadratic Parametric Representation," Comp. and Struct. 16(5), 657-668 (1983).

33. A.B. Sabir, "An Extension of the Shallow to Nonshallow Stiffness Matrix for Cylindrical Shell Finite Element," Int. J. Mech. Sci., 12(3), 287-292 (1970).

34. A.B. Sabir and A.C. Lock, "A Curved Cylindrical Shell Finite Element," Int. J. Mech. Sci., 14 125 (1972).

35. D.G. Ashwell and A.B. Sabir, "A New Cylindrical Shell Finite Element Based on Simple Independent Strain Function," Int. J. Mech. Sci., 14, 171 (1972).

36. G. Cantin and R.W. Clough, "A Curved Cylindrical Shell Finite Element," AIAA Journal, 6, 1057-1062 (1968).

37. D.G. Ashwell and A.B. Sabir, "Limitations of Certain Curved finite Elements when Applied to Arches," Int. J. Mech. Sci., 13, 133-139 (1971).

38. P. Mebane and J. Stricklin, "Implicit Rigid body Motion in Curved Finite Elements," AIAA J. 9(2), 344 (1971).

39. G.A. Fonder and R.W. Clough, "Explicit Addition of Rigid body Motion in Curved Finite Elements," AIAA J., 11, 305 (1973).

40. R.H. MacNeal, "Derivation of Element Stiffness Matrices by Assumed Strain Distributions," Nuclear Engineering and Design, 70, 3-12 (1982).

41. O.C. Zienkiewicz, "Finite Element Method in Engineering Sciences," McGraw-Hill, 1971.

42. E.N. Dvorkin and K.J. Bathe, "A Continuum Mechanics Based Four-Node Shell Element for General Nonlinear Analysis," to appear in Engineering Computations.

43. G. Cantin, "Rigid body motions in curved finite elements," AIAA J., 8, 1252 (1970).

44. J.M. Kennedy and T. Belytschko, "Buckling and Post-buckling Behavior of the ACS Support Columns," Nuclear Engineering and Design, 75, 323-342, (1982).

45. H.A. Balmer and E.A. Witmer, "Theoretical Experimental Correlation of Large Dynamic and Permanent Deformation of Impulsively Loaded Simple Structures," Air Force Flight Dynamic Lab., Rept. FDP-TDR-64-108, Wright-Patterson AFB, Ohio, 1964.

APPENDIX A

The matrices $\underset{\sim}{K}_m$ and $\underset{\sim}{I}$ of Eq. (23) will be presented here in the form consistent with the deformational degrees of freedom given in Eqs. (14b) and (14c).

To obtain the required form of $\underset{\sim}{K}_m$ note that it represents membrane strain energy of the constant-strain, flat triangular element

$$U_m = \frac{1}{2} \int_{\Omega} \underset{\sim}{\varepsilon}^T \underset{\sim}{D} \underset{\sim}{\varepsilon} \, dA \tag{24}$$

where Ω is the area of the element

$$D = \frac{Eh}{(1-\nu^2)} \begin{bmatrix} 1 & \nu & 0 \\ \nu & 1 & 0 \\ 0 & 0 & \frac{1-\nu}{2} \end{bmatrix} \tag{25a}$$

$$\underset{\sim}{\varepsilon}^T = [\varepsilon_x, \varepsilon_y, \gamma_{xy}] \tag{25b}$$

For a constant strain triangle it is natural to replace ε_x, ε_y, γ_{xy} with strains along each of its sides ε_I. Since

$$\varepsilon_I = \frac{\eta_I}{\ell_I} \quad , \qquad I = 1, 2, 3 \tag{26}$$

and

$$\varepsilon_I = \varepsilon_x \, e_{Ix}^2 + \varepsilon_y \, e_{Iy}^2 + \gamma_{xy} \, e_{Ix} \, e_{Iy} \tag{27}$$

we obtain

$$\underset{\sim}{\varepsilon} = \underset{\sim}{S}^{-1} \underset{\sim}{n} \tag{28}$$

where

$$\underset{\sim}{S} = \begin{bmatrix} \ell_1 e_{1x}^2 & \ell_1 e_{1y}^2 & \ell_1 e_{1x} e_{1y} \\ \ell_2 e_{2x}^2 & \ell_2 e_{2y}^2 & \ell_2 e_{2x} e_{2y} \\ \ell_3 e_{3x}^2 & \ell_3 e_{3y}^2 & \ell_3 e_{3x} e_{3y} \end{bmatrix} \tag{29}$$

ℓ_I is the length of side I and e_{Ix}, e_{Iy} are x and y components of the vector $\underset{\sim}{e}_I$ (Fig. 2). In view of Eqs. (24) and (28) the desired form of the matrix $\underset{\sim}{K}_m$ is

$$\underset{\sim}{K}_m = A(\underset{\sim}{S}^{-1})^T \underset{\sim}{D}\, \underset{\sim}{S}^{-1} \tag{30}$$

To obtain the matrix $\underset{\sim}{I}$ of Eq. (22) we observe that it defines the elongation n_I^b of each of the curved sides of the element due to inextensional

$$T = \begin{bmatrix} -\ell_1 c_2^1 e_{1y} & \ell_1 c_2^1 e_{1x} & 0 & 0 & -\ell_1 c_1^1 e_{iy} & \ell_1 e_1^1 e_{1x} \\ -\ell_2 c_1^2 e_{2y} & \ell_1 c_1^2 e_{2x} & -\ell_2 c_2^2 e_{2y} & \ell_2 c_2^2 e_{2x} & 0 & 0 \\ 0 & 0 & -\ell_3 c_1^3 e_{3y} & \ell_3 c_1^3 e_{3x} & -\ell_3 c_2^3 e_{3y} & \ell_3 c_2^3 e_{3x} \end{bmatrix} \tag{31}$$

where

$$c_1^I = \frac{2}{15}\alpha_1^I - \frac{1}{30}\alpha_2^I \tag{32a}$$

$$c_2^I = \frac{2}{15}\alpha_2^I - \frac{1}{30}\alpha_1^I \tag{32b}$$

TABLE 1

Displacement of loaded point in Circular Arch, Example 1

number of elements	NDOF	Flat element (DKT)		Curved element (DKT)	
		$\bar{u}$	$\bar{v}$	$\bar{u}$	$\bar{v}$
4	9	0.482	0.307	0.994	1.127
8	18	0.256	0.230	1.035	1.038
12	27	0.301	0.287	1.007	1.008
16	36	0.398	0.388	1.002	1.003

Horizontal and vertical deflection, $\bar{u}$ and $\bar{v}$, are normalized with respect to analytic solution.

TABLE 2

Deflection for thicker pinched cylinder*

mesh on octant	curved		flat		Cantin [43]	Ashwell and Sabir [35]	Thomas and Gallagher [19]	Bogner et al. [45]	Cantin and Clough [36]
	DKT	C^0 [4]	DKT	C^0 [4]					
1 x 1						0.913	0.042	0.022	
1 x 2	1.010	1.028	0.940	0.970				0.704	0.261
1 x 4	1.011	1.073	0.996	1.054		0.971	0.972	0.954	0.675
1 x 8	0.988	1.043	0.989	1.039			0.982		0.867
2 x 2	0.915	0.870	0.837	0.814	0.817	0.968		0.709	0.928
4 x 4	0.970	0.956	0.939	0.926	0.989	0.991			0.942
6 x 6	0.985	0.978	0.970	0.963	0.998	0.996			0.990
8 x 8	0.991	0.987	0.982	0.978	1.000	0.999			
10 x 10	0.994	0.990	0.989	0.985	1.000	0.998			

* Results are normalized to solution of Cantin [43], 0.1139, thickness 0.094

TABLE 3

Deflection for thin pinched cylinder*

mesh on octant	curved		flat		Ashwell and Sabir [35]	Thomas and Gallagher [15]	Cantin and Clough [36]	Sabir and Lock [34]
	DKT	C^0 [4]	DKT	C^0 [4]				
1 x 1						0.001	0.000	0.000
1 x 2	1.054	1.072	0.982	1.012		0.649		
1 x 4	1.050	1.112	1.031	1.089	0.985	0.954	0.030	0.026
1 x 6	1.030	1.092	1.026	1.080		1.000		
1 x 8	1.019	1.075	1.022	1.069	0.986	1.011	0.287	0.283
2 x 8	1.023	1.036	1.015	1.028	0.990		0.287	0.285
3 x 8	1.018	1.022	1.009	1.013	0.991		0.287	0.285
8 x 8	1.003	1.000	0.995	0.991	0.997		0.290	0.289

* Results are normalized with respect to solution of [35]: 0.02439; thickness = 0.01548

TABLE 4

Deflection Under Point Load for Pinched Cylinder with End Diaphragm*

mesh on octant	degrees of freedom	DKT		Dvorkin and Bathe [42]
		curved	flat	
2 x 2	22	1.324	0.054	-
4 x 4	84	0.777	0.462	-
5 x 5	130	-	-	0.51
6 x 6	186	0.869	0.727	-
8 x 8	328	0.948	0.860	-
10 x 10	510	0.988	0.930	0.83

* Results are normalized by exact solution, 0.18248×10^{-4}.

TABLE 5

Material and geometric constants for impulsively loaded cylindrical panel

Young's modulus	$E = 10.5 \times 10^6$
Density	$\rho = 2.5 \times 10^{-4}$ lb-sec^2/in^4
Poisson's ratio	$\nu = 0.33$
Yield stress	$\sigma = 44000.$ psi
Plastic modulus	$E_p = 0.$ psi
Impulse over R_I	5650 in/sec

TABLE 6

Final Displacements of the Cylindrical Panel
for Various Meshes with Ilyushin Field Condition

Mesh for Half-panel	Displacement at y = 6.28	Displacement at y = 9.42	CPU tim IBM 3033
6 x 16	0.917	0.401	33
8 x 16	1.043	0.448	138
10 x 20	1.081	0.462	162
12 x 24	1.124	0.473	291
16 x 32	1.183	0.530	670
experimental [46]	1.28	0.70	

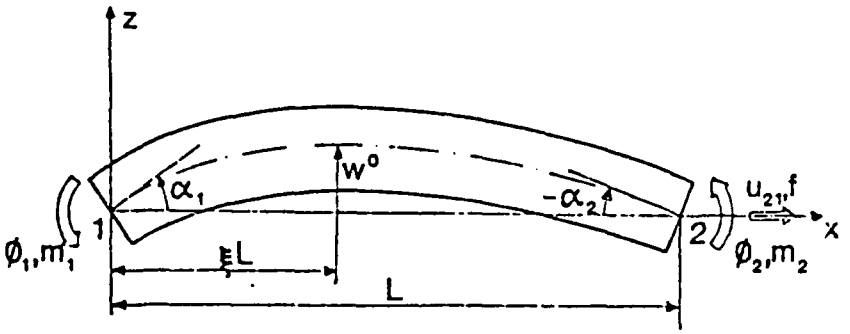

Figure 1. Curved beam nomenclature.

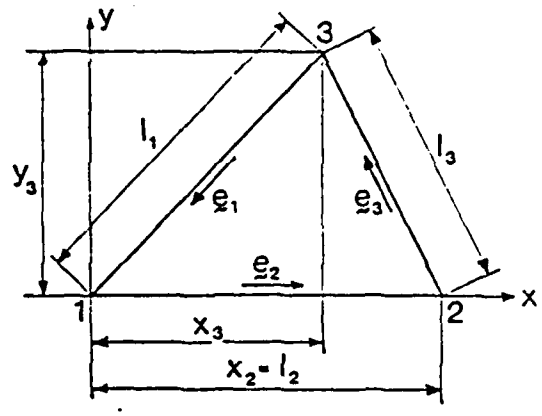

Figure 2. Nomenclature and coordinate system for shell element.

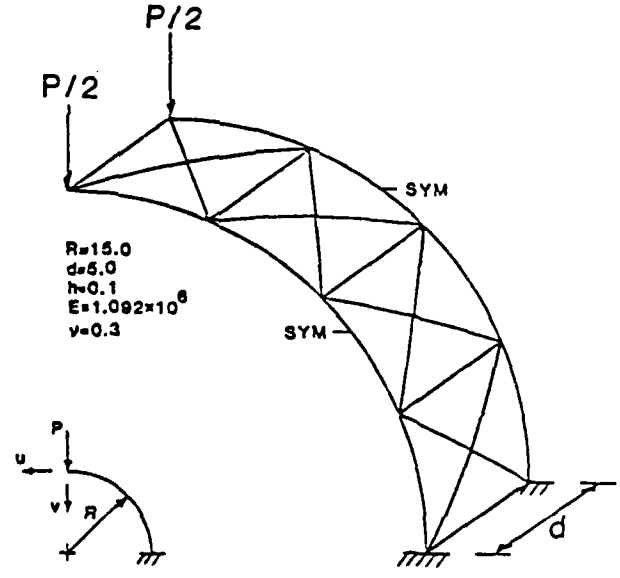

Figure 3. Example 1. Bending of an infinite cylindrical Shell.

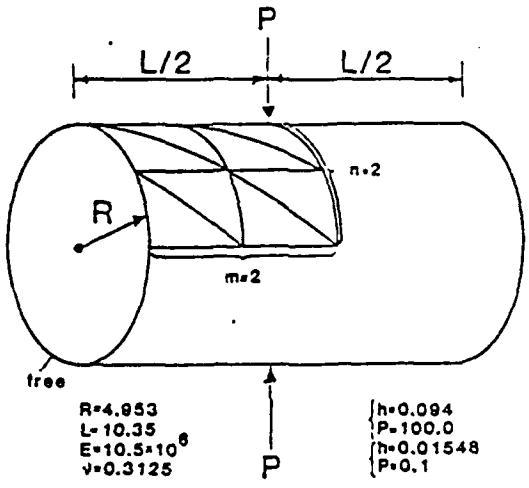

Figure 4. Example 2. Pinched cylinder with free edges.

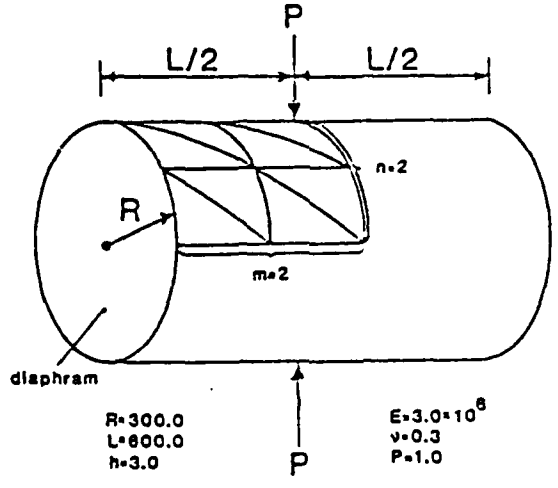

Figure 5. Example 3. Pinched cylinder with end diaphragms.

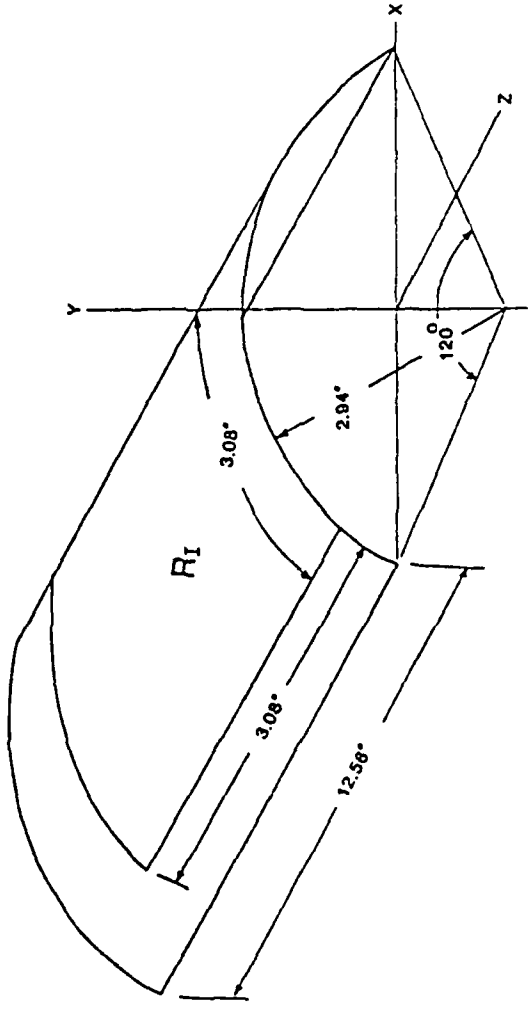

Figure 3. Impulsively loaded cylindrical panel .

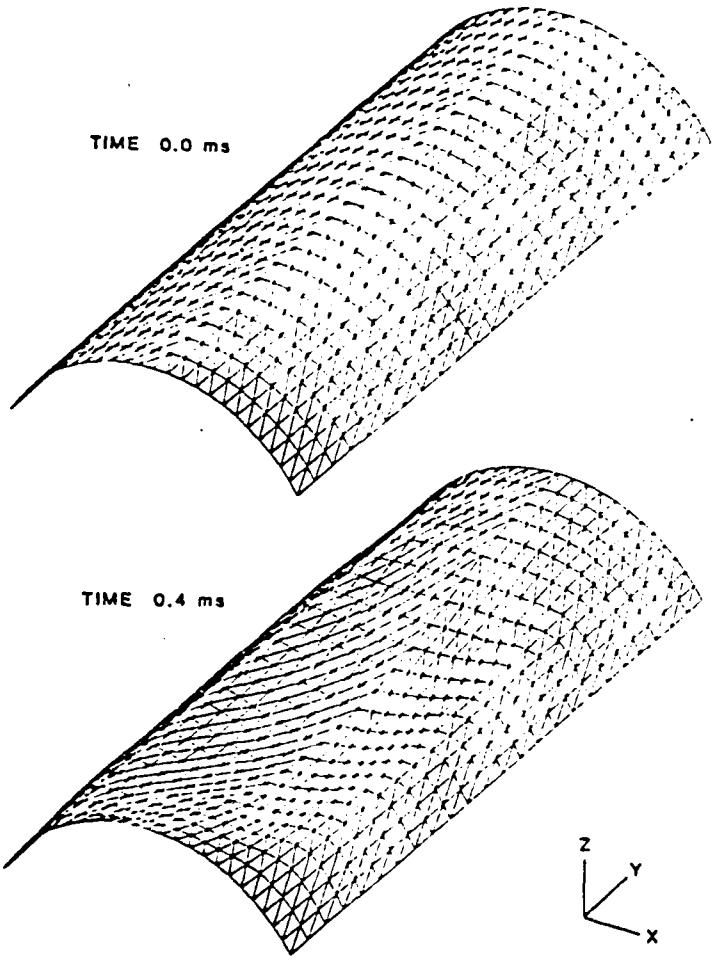

Figure 7. Deformed mesh for cylindrical panel.

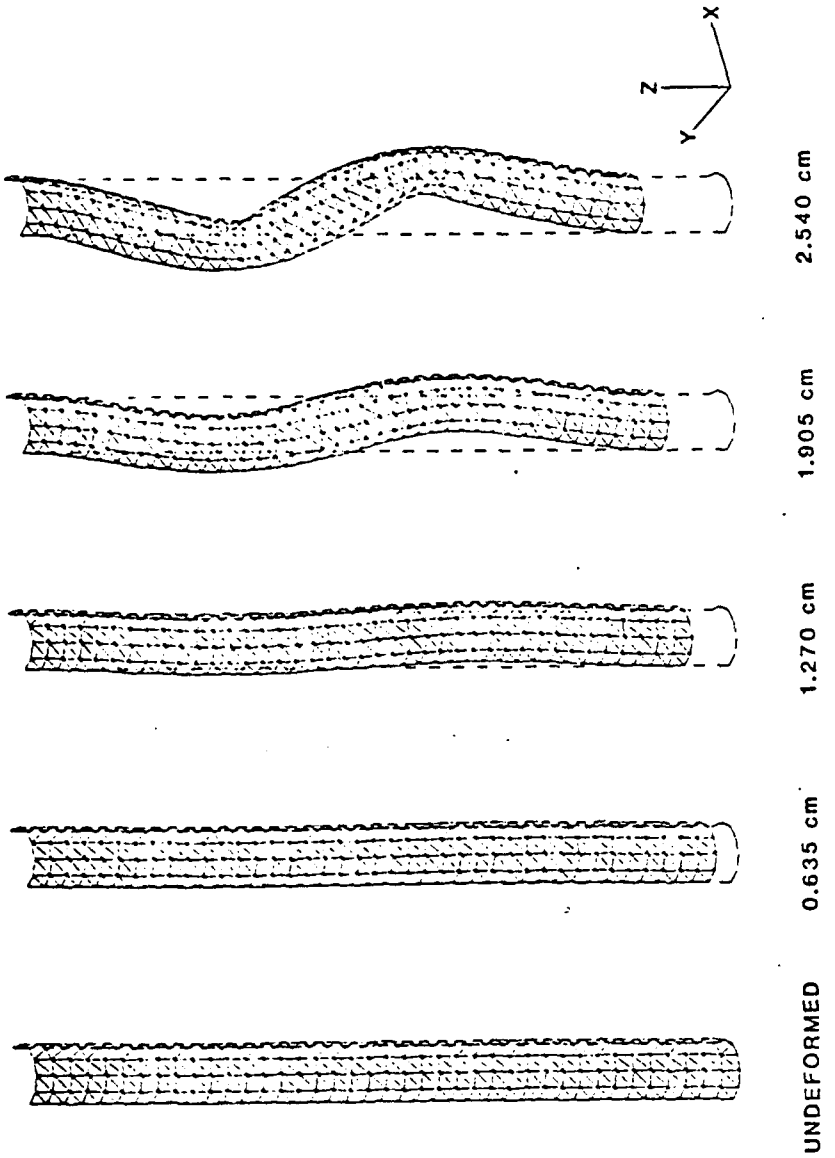

Figure 8. Underformed and deformed meshes for axially loaded hollow column.

CHAPTER 2
SINGULAR MODE CONTROL IN 9 NODE PLATE ELMENT

1. Introduction

The numerical quadrature of higher order elements is a critical issue which must be treated with considerable care. It was recognized by Zienkiewicz et al [1] that in order to obtain reasonable rates of convergence for C^0 plate and shell elements, reduced integration of the shear terms is a necessity. Recently it has become clear that for curved elements, overintegration of the membrane terms [2-5] also impairs convergence; this phenomenon has been termed membrane locking. In fact, this phenomenon also occurs in the application of continuum elements to curved members [5].

On the other hand, reduced integration leads to the appearance of spurious singular modes, and several of the elements which have appeared in the literature for plate analysis cannot treat the modal analysis of unsupported plates because they rely on boundary conditions to suppress these spurious modes; see for example the results in [6] on the plate element of [7]. These modes are also known as kinematic modes, spurious zero-energy modes, and for the 4-node quadrilateral, as hourglass or keystone modes.

In the 4 node continuum and plate elements, considerable progress has recently been achieved in controlling hourglass modes. Kosloff and Frazier [8] first recognized that in controlling spurious singular modes, care must be taken to ensure that the resulting element will pass the patch test and not adversely affect rigid body and constant strain patterns. While the method of [8] involved the solution of systems of equations, in [9-10] explicit forms of the operators for controlling singular modes were developed. In [11], these forms were derived from the consistency conditions (which are equivalent to the patch test [12]). This, in constrast to [8], makes the development of simple, explicit forms of the spurious mode control feasible for a large class

of elements; by using a mixed variational principle, the identification of control parameters for nonlinear materials was also achieved. Applications of these concepts to the diffusion equation, plate, and shell problems are given in [12-14], respectively. The development of plate elements of proper rank has also been undertaken via hybrid [15] and mixed formulations [16].

In this paper, the consistency conditions will be used to derive a spurious mode control for the 9 node Lagrange element. Pawsey [17] evidently first noted their appearance in higher order elements. Shortly thereafter, Cook [18] proposed a control which consisted of simply adding a spring between the center nodes of all elements and a fixed point. This method obviously would not pass the patch test, but its performance in simple problems is not bad. The presence of spurious singular modes in the 9-node Lagrange elements with 2 x 2 quadrature was demonstrated numerically in continuum elements and the diffusion equation in [19] and [20], respectively. Cook and Zhao-hua [21] have proposed a control method which consists of perturbing the 9-node stiffness by that of the 8-node serendipity element. This element passes the patch test but requires condensation of the interior node, which is awkward for nonlinear applications.

In this paper, a method for controlling (or stabilizing) the spurious singular modes by using the consistency conditions in the manner of [11] is developed. The control is first developed for the diffusion operator because it is the simplest setting in which these modes appear; Section 2 gives the discrete form of the diffusion equation to be used here. Section 3 describes the spurious mode control procedure and Section 4 gives results for selected problems. The important feature of these results is that with 2 x 2 quadrature of the 9-node element and hourglass control, the convergence rate of

the element in the L_2-norm is still almost h^3 for straight sided elements.

In Sections 5 and 6, the Mindlin type plate element and the appropriate stabilization procedure are developed, respectively. In this setting, reduced quadrature is imperative because full quadrature results in locking. Results are given in Section 7, which demonstrate almost h^3 convergence for both curved and straight elements. Conclusions are given in Section 8.

2. Discrete Laplace Equaition With 9 Node Lagrange Element

The Laplace (diffusion) equation is considered in the form

$$(\alpha_{ij}\, u_{,j})_{,i} + s = 0 \tag{2.1}$$

where

u = dependent variable, temperature for heat transfer;

α_{ij} = diffusivity constants, conductivity in the case of heat transfer;

s = source

Standard indicial notation will be used, with lower case indices designating Cartesian components; all repeated indices are summed. Commas denote derivatives with respect to the following variables. All constants and variables are considered functions of x and y.

The dependent variable u and a test function δu is approximated by shape functions $N_I(x,y)$ in each element by

$$u = \sum_{I=1}^{n_N} N_I(x,y)\; u_I^e = \underset{\sim}{N}\, \underset{\sim}{u}^e \tag{2.2}$$

where upper case subscripts refer to node numbers and n_N is the number of nodes possessed by the element. Following standard finite element procedures, the conductance matrix can be shown to be given by

$$\underset{\sim}{K}^e = [K_{IJ}]^e = \int_{\Omega_e} N_{I,i}\, \alpha_{ij}\, N_{J,j}\, d\Omega \tag{2.3}$$

The above is often written in the form

$$\underset{\sim}{K}^e = \int_{\Omega_e} \underset{\sim}{B}^T\, \underset{\sim}{D}\, \underset{\sim}{B}\, d\Omega \tag{2.4}$$

where

$$\underset{\sim}{B} = \begin{Bmatrix} \underset{\sim}{b}_1^T \\ \underset{\sim}{b}_2^T \end{Bmatrix} = \begin{Bmatrix} N_{I,x} \\ N_{I,y} \end{Bmatrix} \tag{2.5a}$$

$$\underset{\sim}{D} = \begin{bmatrix} \alpha_{11} & \alpha_{12} \\ \alpha_{12} & \alpha_{22} \end{bmatrix} \tag{2.5b}$$

where the symmetry of the coefficients α_{ij} has been invoked; $\underset{\sim}{B}$ is called the discrete form of the gradient operator since (see Eqs. (2.2) and (2.5a))

$$u_{,i} = \sum_{I=1}^{n_N} B_{iI}\, u_I^e = \underset{\sim}{b}_i^T\, \underset{\sim}{u}^e \tag{2.6}$$

and the transpose of $\underset{\sim}{B}$ is the discrete form of the divergence operator.

For the 9-node Lagrange element, the shape functions N_I are

$$N_I = \mathcal{L}_J(\xi)\, \mathcal{L}_K(\eta) \qquad I = 3(J-1) + K \tag{2.7}$$

where $\mathcal{L}_J(\xi)$ are the standard one-dimensional Lagrange interpolation functions in terms of the reference coordinates ξ,η (see Fig. 1) over the points (-1, 0, +1) which are

$$\mathcal{L}_1(\xi) = \frac{1}{2}\,\xi\,(\xi - 1)$$

$$\mathcal{L}_2(\xi) = 1 - \xi^2 \tag{2.8}$$

$$\mathcal{L}_3(\xi) = \frac{1}{2}\,\xi\,(\xi+1)$$

The reference plane is related to the physical plane by

$$x_i = \sum_{I=1}^{n_N} N_I\, x_{iI} = \underset{\sim}{N}\, \underset{\sim}{x}_i \tag{2.9}$$

where x_{iI} are the coordinates of node I; the nodal coordinates are sometimes arranged in 2 column matrices $\underset{\sim}{x}_i$, where $\underset{\sim}{x}_1 = \underset{\sim}{x}$, $\underset{\sim}{x}_2 = \underset{\sim}{y}$.

When numerical quadrature is used, the conductance matrix, Eq. (4), is evaluated by

$$\underset{\sim}{K}^e = \sum_{\alpha=1}^{n_G} \rho_\alpha\, \underset{\sim}{B}^T\,(\underset{\sim}{x}^Q_\alpha)\, \underset{\sim}{D}\,(\underset{\sim}{x}_\alpha)\, \underset{\sim}{B}\,(\underset{\sim}{x}^Q_\alpha) \tag{2.10}$$

where $\underset{\sim}{x}^Q_\alpha = (x^Q_\alpha, y^Q_\alpha)$, $\alpha = 1$ to n_G, are the quadrature (integration) points and ρ_α the quadrature weights including the Jacobian. The above can be written as

$$\underset{\sim}{K}^e = \underset{\sim}{B}^T \underset{\sim}{D} \underset{\sim}{B} \tag{2.11}$$

where

$$\overline{\underset{\sim}{B}} = \begin{Bmatrix} \underset{\sim}{B}(x_1^Q) \\ \underset{\sim}{B}(x_2^Q) \\ \vdots \\ \underset{\sim}{B}(x_{n_G}^Q) \end{Bmatrix} \tag{2.12}$$

$$\overline{\underset{\sim}{D}} = \begin{bmatrix} \rho_1 \underset{\sim}{D}(x_1^Q) & \underset{\sim}{0} & & \underset{\sim}{0} \\ & \rho_2 \underset{\sim}{D}(x_2^Q) & & \underset{\sim}{0} \\ & \cdots\cdots\cdots & & \\ & & & \rho_{n_G} \underset{\sim}{D}(x_{n_G}^Q) \end{bmatrix} \tag{2.13}$$

Consider the quadrature scheme indicated in Fig. 1. Using Eq. (5a), and using the notation $\underset{\sim}{b}_{i\alpha} = b_i(x_\alpha^Q)$, $\overline{\underset{\sim}{B}}$ can be written for 2 x 2 quadrature as

$$\bar{\underset{\sim}{B}} = \begin{Bmatrix} \underset{\sim}{b}_1^T(\underset{\sim}{x}_1^Q) \\ \underset{\sim}{b}_2^T(\underset{\sim}{x}_1^Q) \\ \vdots \\ \underset{\sim}{b}^T(\underset{\sim}{x}_4^Q) \end{Bmatrix} = \begin{Bmatrix} \underset{\sim}{b}_{11}^T \\ \underset{\sim}{b}_{21}^T \\ \vdots \\ \underset{\sim}{b}_{24}^T \end{Bmatrix} \tag{2.14}$$

The rank of $\underset{\sim}{K}^e$ is at most equal to the rank of $\bar{\underset{\sim}{B}}$. This is a consequence of the fact that the dimension of the null-space of $\bar{\underset{\sim}{B}}$ is equal to that of the null-space of $\underset{\sim}{K}^e$ because if $\bar{\underset{\sim}{B}}\ \underset{\sim}{u} = \underset{\sim}{0}$, then $\underset{\sim}{K}^e\ \underset{\sim}{u} = \underset{\sim}{0}$; see Eq. (2.11). With this quadrature scheme the rank of $\bar{\underset{\sim}{B}}$ could be at most 8, since $\bar{\underset{\sim}{B}}$ has 8 rows; however one of these 8 rows is a linear combination of the other 7, so the rank of $\bar{\underset{\sim}{B}}$ and $\underset{\sim}{K}^e$ is 7; this rank deficiency has also been reported in [20].

3. Spurious Mode Control for Laplace Equation

The essential feature of an effective control of spurious singular modes is that the stabilization matrix should not result in a violation of the consistency conditions. The consistency conditions, which are in a sense equivalent to the patch test [22, 23] require that

$$\underset{\sim}{b}_{i\alpha}^T\ \underset{\sim}{x}_j = \delta_{ij} \qquad \text{for all } \alpha \tag{3.1}$$

$$\underset{\sim}{b}_{i\alpha}^T\ \underset{\sim}{s} = 0 \quad \text{or} \quad \bar{\underset{\sim}{B}}\ \underset{\sim}{s} = \underset{\sim}{0} \tag{3.2}$$

where

$$\underset{\sim}{s} = [1, 1, 1, 1, 1, 1, 1, 1, 1] \tag{3.3}$$

Equations (3.1) and (3.2) were verified algebraically for rectangular elements and numerically for a large variety of curved elements.

Note that Eq. (3.1) corresponds to the requirement that $x_{i,j} = \delta_{ij}$ (cf. Eqs. (2.5a), (2.9)), i.e. that the gradient of a linear field be computed exactly, while Eq. (3.2) implies that any constant field has a zero gradient. Using Eq. (2.11), Eq. (2.16) can be seen to imply that

$$\underset{\sim}{K}^e \underset{\sim}{s} = \underset{\sim}{0} \tag{3.4}$$

Thus $\underset{\sim}{s}$ is in the null-space of $\bar{\underset{\sim}{B}}$ and $\underset{\sim}{K}^e$. The vector space spanned by $\underset{\sim}{s}$ is called the proper null-space of $\underset{\sim}{K}^e$ because the gradient is expected to vanish for a constant field $u(x,y)$ which is associated with the nodal values $\underset{\sim}{u}^e = \underset{\sim}{s}$.

It can also be shown that

$$\underset{\sim}{b}_{i\alpha}^T \underset{\sim}{h} = 0 \quad \text{or} \quad \bar{\underset{\sim}{B}} \underset{\sim}{h} = \underset{\sim}{0} \tag{3.5}$$

$$\underset{\sim}{K}^e \underset{\sim}{h} = \underset{\sim}{0} \tag{3.6}$$

where

$$\underset{\sim}{h} = [+1, -1, +1, -1, 0, -1, +1, -1, +1] \tag{3.7}$$

Equation (3.5) has been verified algebraically for rectangular elements and

checked numerically for a large number of rhombic and curved elements; Eq. (3.6) follows from (3.5) because of Eq. (2.11). The one-dimensional vector space of $\underset{\sim}{h}$ is called the improper null-space of $\overline{\underset{\sim}{B}}$ because the gradient of the function u associated with the nodal values $\underset{\sim}{u}^e = \underset{\sim}{h}$ is obviously not zero, as can be seen from a depiction of this mode in Fig. 2.

Simple examination of Eqs. (3.3) and (3.7) reveals that the vector $\underset{\sim}{h}$ is also orthogonal to $\underset{\sim}{s}$, i.e.

$$\underset{\sim}{h}^T \underset{\sim}{s} = 0 \tag{3.8}$$

so that the entire complement to the proper null space of $\underset{\sim}{s}$ is spanned by the 9 vectors $\underset{\sim}{b}_{i\alpha}$ and $\underset{\sim}{h}$.

The control of the improper (spurious) mode is accomplished by defining an additional generalized gradient $\tilde{g}$ by

$$\tilde{g} = \underset{\sim}{\chi}^T \underset{\sim}{u}^e \tag{3.9a}$$

and a generalized flux by

$$\tilde{q} = - \tilde{\alpha}\, \tilde{g} \tag{3.9b}$$

where the determination of $\tilde{\alpha}$ is described later.

The resulting element conductance matrix is then given by

$$\underset{\sim}{K}^e = \overline{\underset{\sim}{B}}^T \overline{\underset{\sim}{D}}\, \overline{\underset{\sim}{B}} + \tilde{\alpha}\, \underset{\sim}{\chi}\, \underset{\sim}{\chi}^T \tag{3.10}$$

where the second term in the above is the stabilization matrix [6,12].

If the above stiffness matrix is to meet the consistency requirements on linear fields, it is sufficient and necessary that $\tilde{g}$ vanish for any nodal values associated with the linear field [11]

$$u = c_o + c_1 x + c_2 y = c_o + c_i x_i \tag{3.11a}$$

that is, for nodal values of $\underset{\sim}{u}$ given by

$$\underset{\sim}{u} = c_o \underset{\sim}{s} + c_i \underset{\sim}{x}_i \tag{3.11b}$$

the generalized gradient $\tilde{g}$ must vanish. This is equivalent to the requirement that

$$\chi^T (c_o \underset{\sim}{s} + c_i \underset{\sim}{x}_i) = 0 \tag{3.12}$$

for all c_i, i = 0 to 2. Since the 10 vectors $\underset{\sim}{b}_{i\alpha}$, $\underset{\sim}{s}$ and $\underset{\sim}{h}$ span the 9 dimensional vector space R^9, the most general form of χ is given by

$$\chi = \sum_{\alpha=1}^{4} [a_{1\alpha} \underset{\sim}{b}_{1\alpha} + a_{2\alpha} \underset{\sim}{b}_{2\alpha}] + a_9 \underset{\sim}{h} + a_{10} \underset{\sim}{s} \tag{3.13}$$

Substituting the above into Eq. (3.12) and using Eqs. (3.1) (3.2), (3.5) and (3.8) yields

$$c_0(a_{10}\,\underset{\sim}{s}^T\,\underset{\sim}{s}) + c_1(a_9\underset{\sim}{h}^T\underset{\sim}{x} + a_{10}\underset{\sim}{s}^T\underset{\sim}{x} + \sum_{\alpha=1}^{4}\alpha_{1\alpha}) + c_2(a_9\underset{\sim}{h}^T\underset{\sim}{y} + a_{10}\underset{\sim}{s}^T\underset{\sim}{y} + \sum_{\alpha=1}^{4}a_{2\alpha}) = 0 \qquad (3.14)$$

Since the above must hold for all c_i, it follows that

$$a_{10} = 0 \qquad (3.15a)$$

$$a_9\,\underset{\sim}{h}^T\underset{\sim}{x} + \sum_{\alpha=1}^{4} a_{1\alpha} = 0 \qquad (3.15b)$$

$$a_9\,\underset{\sim}{h}^T\underset{\sim}{y} + \sum_{\alpha=1}^{4} a_{2\alpha} = 0 \qquad (3.15c)$$

Equations (3.15) represent 2 conditions on the 8 parameters $a_{i\alpha}$. Therefore considerable leeway is available in the choice of these constants if consistency is only required with respect to linear fields. It can be met by letting

$$a_{1\alpha} = -\frac{1}{4}\,a_9\underset{\sim}{h}^T\underset{\sim}{x}, \qquad \alpha = 1 \text{ to } 4 \qquad (3.16a)$$

$$a_{2\alpha} = -\frac{1}{4}\,a_9\underset{\sim}{h}^T\underset{\sim}{y}, \qquad \alpha = 1 \text{ to } 4 \qquad (3.16b)$$

which with Eqs. (3.13) and (3.15) gives

$$\underset{\sim}{\chi} = \underset{\sim}{h} - \frac{1}{4}\left[(\underset{\sim}{h}^T\underset{\sim}{x})\sum_{\alpha=1}^{4}\underset{\sim}{b}_{1\alpha} + (\underset{\sim}{h}^T\underset{\sim}{y})\sum_{\alpha=1}^{4}\underset{\sim}{b}_{2\alpha}\right] \qquad (3.17)$$

The common constant a_9 has been omitted.

For purposes of constructing the stabilization matrix, (3.10), the constant $\tilde{\alpha}$ is expressed in terms of a stabilization parameter ε by

$$\tilde{\alpha} = \frac{\varepsilon \alpha_{ii}}{200} \sum_{\alpha=1}^{4} \rho_\alpha \, \underset{\sim}{b}_{i\alpha}^T \, \underset{\sim}{b}_{i\alpha} \tag{3.18}$$

In this form $\varepsilon = 1$ closely approximates the exactly integrated matrix for rectangles when $\underset{\sim}{\alpha}$ is isotropic.

Remark. This procedure involves 8 arbitrary constants, $a_{1\alpha}$ and $a_{2\alpha}$, so it would be advantageous if consistency of the quadratic and biquadratic polynomials could also be enforced. However, the resulting consistency equations are singular and we have not been able to circumvent this difficulty. Furthermore, quadratic consistency is not satisfied by the 9-node element when the element is not a parallellogram, that is,

$$\underset{\sim}{b}_{i\alpha}^T \, \underset{\sim}{u} \neq u_{,i}(\underset{\sim}{x}_\alpha^Q) \tag{3.19}$$

when u is a quadratic function of (x,y) and $\underset{\sim}{u}$ are its nodal values.

Remark: Equation (3.17) can also be written in a form easily implemented on a computer as follows

$$\gamma_I = h_I - \frac{1}{4}\left[h_x \sum_{\alpha=1}^{4} B_{1I}(\underset{\sim}{x}_\alpha^Q) + h_y \sum_{\alpha=1}^{4} B_{2I}(\underset{\sim}{x}_\alpha^Q)\right] \tag{3.20}$$

where

$$h_x = \underset{\sim}{h}^T \underset{\sim}{x} \qquad h_y = \underset{\sim}{h}^T \underset{\sim}{y} \tag{3.21}$$

and $\underset{\sim}{x}_\alpha^Q$ are the 4 quadrature points.

4. Numerical Examples for the Laplace Equation

Several problems were solved for the purpose of examining the performance of this spurious mode control procedure, with particular emphasis on the rates of convergence and the effects of varying the parameter ε. All of the problems solved were linear and, except for one, steady-state. For simplicity, the dependent variable u is called the temperature throughout this section.

Example 1 is defined in Fig. 3. Three meshes were used for this problem. The temperature distribution along the axis B-C is compared with the analytic solution in Fig. 4. Figure 5 shows the results for the fine mesh with ε = 0.1 and 1.0, respectively. It can be seen that in this problem the effect of the stabilization parameter ε is minimal. Because this problem has a prescribed temperature along all boundaries (Dirichlet type), 2 x 2 quadrature without stabilization does not lead to any spurious modes, so these solutions primarily show that the introduction of this spurious mode control procedure does not distort the solution.

Example 2 is described in Fig. 6. Again, three meshes were used as shown in Fig. 6. Four-fold symmetry was used in these problems and the lines of symmetry are considered insulated, i.e. the gradient vanishes along the lines x = 0 and y = 0. Since this is a natural boundary condition, it need not be explicitly enforced. The solutions for three different values of ε are given

in Fig. 7. This problem, because of the shortage of essential boundary conditions, can exhibit spurious modes, and as can be seen, for the lowest values of ε, oscillations in the temperature u are quite clear. For $\varepsilon = 1.0$, the oscillations are almost completely eliminated and the solution agrees well with the analytic solution. Note that the results with insufficient stabilization do not oscillate about the correct solution.

Example 3 is identical to example 2 except that a Dirichlet boundary condition is applied to the circumference, see Fig. 6. Results for the three meshes in Fig. 6 are given in Fig. 8, and compared to the analytic solution; results for two values of ε are given in Fig. 9. Both agree well with the analytic solution.

Figure 10 shows the L_2 norm of error as a function of element size h for examples 1 and 3, which are rectangular and circular domains, respectively. The L_2 norm was computed by evaluating

$$E^2 = \sum_{e=1}^{n_e} \int_{\Omega_e} \left(u^{FEM} - u^{analytic}\right)^2 d\Omega$$

and 5 x 5 quadrature was used to evaluate the above integral in each element. Results for both the stabilization procedure with $\varepsilon = 1$ and 3 x 3 quadrature are given. For the square domain, where the elements are all straight sided, the slope of this curve is 2.95 for both the stabilization procedure and 3 x 3 quadrature. Thus, for this case the stabilization procedure has no undesirable effects on the rate of convergence. In the circular domain, example 3, where some of the elements are curved and irregular, the situation is more complex. For the meshes studied, the absolute accuracy of 3 x 3 quadrature is better than that of stabilization procedure. However, 3 x 3 quadrature exhi-

bits a definite reduction in the rate of convergence with decreasing element size which is absent in the stabilized element. Average slopes are 1.9 for 2x2 with stabilization, 1.4 for 3 x 3 quadrature, so for these irregular meshes, neither 3 x 3 quadrature nor the stabilization procedure retains the optimal h^3 convergence of this element. The results for even higher order quadrature, 4 x 4 and 5 x 5, are almost identical to that for 3 x 3 quadrature.

Figure 11 is included to show the effect of spurious modes more dramatically. In this problem, a circular domain with an insulated outer boundary was considered. A point source which is a step function in time is applied at the center of the domain. The time step in this problem is one, and evidence of spurious oscillations is quite clear within 20 time steps. Within 40 time steps, the entire solution is dominated by the spurious oscillations. Note that in this plot all nodes are connected by solid lines, so each 9-node element is represented by 4 adjacent elements in Fig. 11.

5. Discrete C^0 Plate Equations

The general theory for C^0 plates, which are often called Mindlin plates, is presented in [24]. In this theory, the deformation of the plate is described by three dependent variables; a transverse deflection $w(x,y)$ and rotations $\theta_x(x,y)$ and $\theta_y(x,y)$. The element has 9 nodes with 3 degrees of freedom per node and the three fields are approximated in the element by the 9 shape functions, Eqs. (2.7 - 2.8) in the form

$$w(x,y) = \sum_{I=1}^{n_N} N_I w_I = \underline{N}\,\underline{w} \qquad (5.1)$$

$$\theta_x(x,y) = \sum_{I=1}^{n_N} N_I \theta_{xI} = \underset{\sim}{N}\, \underset{\sim}{\theta}_x \tag{5.2a}$$

$$\theta_y(x,y) = \sum_{I=1}^{n_N} N_I \theta_{yI} = \underset{\sim}{N}\, \underset{\sim}{\theta}_y \tag{5.2b}$$

The element stiffness matrix $\underset{\sim}{K}^e$ is given by

$$\underset{\sim}{K}^e = \int_{A^e} \underset{\sim}{B}_b^T \underset{\sim}{D}_b \underset{\sim}{B}_b \, dA + \int_{A^e} \underset{\sim}{B}_s^T \underset{\sim}{D}_s \underset{\sim}{B}_s \, dA \tag{5.3}$$

bending stiffness shear stiffness

where A^e is the area of element e, and

$$\underset{\sim}{B}_b = \begin{bmatrix} \underset{\sim}{0} & \underset{\sim}{0} & \underset{\sim}{N}_{,x} \\ \underset{\sim}{0} & -\underset{\sim}{N}_{,y} & \underset{\sim}{0} \\ \underset{\sim}{0} & -\underset{\sim}{N}_{,x} & \underset{\sim}{N}_{,y} \end{bmatrix} \tag{5.4}$$

$$\underset{\sim}{B}_s = \begin{bmatrix} \underset{\sim}{N}_{,x} & \underset{\sim}{0} & \underset{\sim}{N} \\ \underset{\sim}{N}_{,y} & -\underset{\sim}{N} & \underset{\sim}{0} \end{bmatrix} \tag{5.5}$$

$$\underset{\sim}{D}_b = D \begin{bmatrix} 1 & \nu & 0 \\ \nu & 1 & 0 \\ 0 & 0 & \frac{1}{2}(1-\nu) \end{bmatrix} \tag{5.6}$$

$$\underset{\sim}{D}_s = \kappa G h \begin{bmatrix} 1 & 0 \\ 0 & 1 \end{bmatrix} \qquad D = \frac{Eh^3}{12(1 - \nu^2)} \tag{5.7}$$

Here h is the thickness, E is Young's modulus, G is the shear modulus, κ is the shear factor and ν is Poisson's ratio.

This element locks if 3 x 3 quadrature is used for both the bending and shear stiffnesses; therefore selective reduced integration is recommended [24]. In this paper, we will use 2 x 2 quadrature for both the shear and bending stiffness and stabilize the kinematic modes.

For the purpose of analyzing this stiffness, we perform the steps indicated in Section 2 in going from Eq. (2.4) to Eq. (2.10) and write the element stiffness for 2 x 2 quadrature in the form

$$\underset{\sim}{K}_e = \overline{\underset{\sim}{B}}^T \, \overline{\underset{\sim}{D}} \, \overline{\underset{\sim}{B}} \tag{5.8}$$

where

$$\overline{B} = \begin{Bmatrix} \underset{\sim}{B}_b \, (\underset{\sim}{x}_1^Q) \\ \underset{\sim}{B}_s \, (\underset{\sim}{x}_1^Q) \\ \vdots \\ \underset{\sim}{B}_s \, (\underset{\sim}{x}_{n_G}^Q) \end{Bmatrix} \tag{5.9}$$

$$\bar{\underset{\sim}{D}} = \begin{bmatrix} \rho_1 \underset{\sim}{D}_b(\underset{\sim}{x}_1^D) & \underset{\sim}{0} & \cdots & \underset{\sim}{0} \\ \underset{\sim}{0} & \rho_1 \underset{\sim}{D}_s(\underset{\sim}{x}_1^Q) & \cdots & \underset{\sim}{0} \\ \cdots & \cdots & \cdots & \cdots \\ \underset{\sim}{0} & \cdots & \underset{\sim}{0} & \rho_{n_G} \underset{\sim}{D}_s(\underset{\sim}{x}_{n_G}^Q) \end{bmatrix} \tag{5.10}$$

where $\underset{\sim}{x}_\alpha^Q$, $\alpha = 1$ to n_G, are the Gauss quadrature points; in this case $n_G = 4$.

The number of rows in the matrix $\bar{\underset{\sim}{B}}$ is 20 so the rank of $\underset{\sim}{K}^e$ is at most 20; the number of degrees of freedom is 27; (9 nodes x 3 degrees of freedom/per node). Thus, since there are 3 rigid body modes, the rank deficiency of the element stiffness is at least 4. The singular modes are given in Table 1.

6. Spurious Mode Control for Plate Element

The spurious modes which are of principal concern are the w, θ_x and θ_y modes. The process of control is analogous to that in the Laplace equation, except that whereas the singular modes in the Laplace equation can be controlled quite stiffly with values of ε of the order of 1, some of the modes in the plate problem are associated with locking and therefore care must be taken in their control.

For the purpose of the control of these 3 modes, three generalized strains are defined by

$$q_w \equiv q_1 = \underset{\sim}{\chi}_1^T \underset{\sim}{w} \tag{6.1a}$$

$$q_{\theta_x} \equiv q_2 = \chi_2^T \underset{\sim}{\theta}_x \tag{6.1b}$$

$$q_{\theta_y} \equiv q_3 = \chi_3^T \underset{\sim}{\theta}_y \tag{6.1c}$$

The structure of the proper null-space for the plate is more complex than for the diffusion equation; it is spanned by the 3 vectors which are called rigid body modes in Table 1. These vectors include both the linear field vectors $\underset{\sim}{x}_i$ and the constant vector $\underset{\sim}{s}$. In spite of this added complexity, the basic conditions on χ_i can be reduced to those on χ in the diffusion equation:

1. χ_i should not affect linear fields:
2. χ_i should span the complement of the proper null-space.

Therefore, the same procedure as given in Section 3 can be used to develop χ_i and it follows that all three of the χ_i operators are identical and given by Eq. (3.17).

The generalized stresses are given by

$$Q_i = c_i^H q_i \qquad \begin{array}{l}\text{for } i = 1 \text{ to } 3,\\ \text{no sum on } i\end{array} \tag{6.2}$$

where c_i^H are given by

$$c_1^H = \frac{r_w h^2 H D}{A} \tag{6.3a}$$

$$c_2^H = c_3^H = r_\theta H \kappa G h \tag{6.3b}$$

$$H = \frac{1}{100} \int_A \underset{\sim}{b}_i^T \underset{\sim}{b}_i \, dA \tag{6.4}$$

The constant H was herein obtained by 2 x 2 quadrature, but it is likely that estimates of H with sufficient accuracy could more easily be obtained.

The generalized strain q_w, as in the 4 node quadrilateral [13], is associated with locking, so r_w should be small; suggested values are: $0.01 \leq r_w \leq 0.1$. In this range, the results have been found to be almost independent of r_w. The normalization of Eqs. (6.3) allows r_w to be applicable to elements with a wide variety of shapes and aspect ratios, for we have found no locking or evidence of spurious modes with r_w in this range. The generalized strains q_2 and q_3 are not associated with a locking mode, so r_θ is usually chosen of order 1.0.

The element stiffness matrix is given by

$$\underset{\sim}{K} = \underset{\sim}{K}^{(2x2)} + \underset{\sim}{K}^{H} \tag{6.5a}$$

$$\underset{\sim}{K}^{H} = \begin{bmatrix} c_1^H \chi \chi^T & \underset{\sim}{0} & \underset{\sim}{0} \\ \underset{\sim}{0} & c_2^H \chi \chi^T & \underset{\sim}{0} \\ \underset{\sim}{0} & \underset{\sim}{0} & c_3^H \chi \chi^T \end{bmatrix} \tag{6.5b}$$

where $\underset{\sim}{K}^H$ is the stabilization matrix and $\underset{\sim}{K}^{(2x2)}$ the standard element matrix obtained by 2x2 quadrature.

If the degrees of freedom of the element are arranged in the conventional order with all degrees of freedom at each node in sequence, i.e. with

$$\underset{\sim}{d}^T = (w_1, \theta_{x1}, \theta_{y1}, w_2, \ldots . \theta_{x9}, \theta_{y9}) \tag{6.6}$$

then $\underset{\sim}{K}^H$ can be easily computed by the following formula

For I = 1 to 9, J = 1 to 9

$$K^H_{LK} = \begin{cases} c^H_1 \gamma_I \gamma_J & L = 3I - 2, \quad K = 3J - 2 \\ c^H_2 \gamma_I \gamma_J & L = 3I - 1, \quad K = 3J - 1 \\ c^H_3 \gamma_I \gamma_J & L = 3I, \quad K = 3J \end{cases} \tag{6.7}$$

All other K^H_{LK} are zero.

Thus the implementation of this element involves simply the standard computation of the element stiffness by 2 x 2 quadrature, followed by the computation of χ by Eq. (3.17) (or (3.20)) and $\underset{\sim}{K}^H$ by the above.

7. Numerical Examples for Plate

Several problems were solved to examine the performance of this spurious mode control procedure in the plate element.

The first problem, example 5, is a clamped, circular plate of radius R subjected to a uniform load q. Results obtained Mesh B from Fig. 6 for two values of r_w are compared to the analytic solution in Fig. 12. In both cases, the θ - hourglass control, $r_\theta = 1.0$. The results, as can be seen, are independent of r_w in this range, and agree very well with the analytic solution.

Figure 13 shows the results for the same problem with $r_w = 0.1$ for the 3 meshes shown in Fig. 6. Even with the coarse mesh, the results agree well with the analytic solution.

Figure 14 shows the convergence rates for this circular clamped plate problem and a uniformly-loaded square plate problem with clamped supports; the meshes shown in Fig. 3 were used for a quarter of the plate in the square plate problem. The L_2 error is here defined as

$$E^2 = \sum_{e=1}^{n_e} \int_{\Omega^e} \left(w^{FEM} - w^{analytic}\right)^2 d\Omega \qquad (7.1)$$

and 5 x 5 quadrature was used to evaluate the above integral in each element. In all cases, $r_w = 0.1$, $r_\theta = 1.0$.

Several points are of interest:

i) The rate of convergence in w for the stabilization method for the square plate is almost 3.0.

ii) The rate of convergence for the circular plate problem with stabilization is 2.6. While the initial rate with selective-reduced integration is also 2.6, the convergence rate diminishes as the mesh is refined.

iii) The behavior with an inconsistent hourglass control $\chi = \underset{\sim}{h}$, i.e. where the last term in Eq. (3.17) is omitted, is similar to that with selective-reduced integration.

While the improved rate of convergence for the circular plate as compared to the Laplacian on a circular domain may be puzzling at first, it is probably attributable to the omission of the rotations from the error in Eq. (7.1).

The performance of the method in a problem characterized by severe singular modes is shown in Figs. 15 and 16, which is a uniformly-loaded square plate with corner supports, such as that studied in [13]. For small values of r_w, spatial oscillations in w are clearly evident. Figure 16 shows the normalized displacement of a node next to the center for the corner supported

and clamped square plates. Note that as for the 4-node quadrilateral [13], the stabilization procedure gives acceptable results for a large range of r_w, so the results are not sensitive to its selection. The clamped plate locks for large values of r_w but exhibits no modes as r_w tends to zero, whereas the corner supported plate diverges for small r_w but does not lock. Only the intermediate values give acceptable solutions to both problems.

Figure 17 shows the displacements for a circular thick-plate subjected to a point load at its center. The boundaries are clamped and the following parameters were considered: $E = 1.09 \times 10^6$ psi; $\nu = 0.3$; thickness $h = 2$ in; radius $R = 5$ in. Mesh B in Fig. 6 was used.

In this case, 2 x 2 quadrature leads to near singularity of the assembled stiffness, and the results with no stabilization exhibit marked oscillations. Effective suppression of oscillations in this case requires a larger value of r_w (0.1) than in any other problem we have solved, and the displacement at the center is more sensitive to r_w.

Figure 18 shows the results obtained for this element in the well-known "single-element twist" problem [25].

The last well-known difficult problem is the rhombic plate. The two meshes shown in Fig. 19 were considered. Displacements and moments are reported in Figs. 20 and 21.

References

1. O.C. Zienkiewicz, R.L. Taylor and J.M. Too, "Reduced integration techniques in general analysis of plates and shells," Int. J.Num. Meth. Engrg., 3 275-290 (1971)

2. H. Parisch, "A critical survey of the 9-node degenerated shell element with special emphasis on thin shell applications and reduced integration, "Comp. Meth. Appl. Mech. Eng., 20 323-350, 1979.

3. H. Stolarski and T. Belytschko, "Membrane locking and reduced integration for curved elements," J. Applied Mechanics, 49, 172-176, 1982.

4. T.J.R. Hughes and W.K. Liu, "Nonlinear finite element analysis of shells: Part I - Three-Dimensional Shells," Comp. Meth. Appl. Mech. Eng, 26, 331-362, 1981.

5. H. Stolarski and T. Belytschko, "Shear and membrane locking and curved C^0 elements," Comp. Meth. Appl. Mech. Engr., in press.

6. T. Belytschko, C.S. Tsay and W.K. Liu, "A stabilization matrix for the bilinear Mindlin plate element," Comp. Meth. in Appl. Mech. and Eng., 29, 313-327, 1981.

7. T.J.R. Hughes, R.L. Taylor and W. Kanoknukulchai, "A simple and efficient finite element for plate bending, Int. J. Num. Meth. Engng., 11, 1529-1547, 1977.

8. D. Kosloff and G. Frazier, "Treatment of hourglass patterns in low order finite element codes," Num. Anal. Meth. Geomech., 2, 52-57 1978.

9. D. Flanagan and T. Belytschko, "A uniform strain hexahedron and quadrilateral with orthogonal hourglass control," Int. J. Num. Meth. Engrg., 17, 679-706 1981.

10. T. Belytschko, "Correction of Article by D.P. Flanagan and T. Belytschko," Int. Journal for Num. Methods in Engrg., Vol. 19, 467-468 1983.

11. T. Belytschko, W.K. Liu, J. Kennedy and J. S-J. Ong, "Hourglass control for linear and nonlinear problems," Recent Developments in Linear and Nonlinear Finite Element Methods, ed. by S. Atluri and N. Perrone, ASME, 1983.

12. W.K. Liu and T. Belytschko, "Efficient Linear and Nonlinear Heat Conduction with a Quadrilateral Element," to be published Int. J. Num. Methods Engrg.

13. T. Belytschko and C-S. Tsay, "A stabilization procedure for the quadrilateral plate element with one-point quadrature," Int. J. Num. Meth. Engrg., 19, 405-419 1983.

14. T. Belytschko, C-S. Tsay and J.I. Lin, "Explicit algorithms for the nonlinear dynamics of shells," Finite Elements for Nonlinear Shells, ed. by T.J.R. Hughes, et al, ASME, 1982 also to appear CMAME.

15. R.L. Spilker, "Invariant 8-node hybrid-stress elements for thin and moderately thick plates," Int. J. Num. Meth. Engrg., 18, 1153-1178 1982.

16. A.K. Noor and C.M. Andersen, "Mixed models and reduced/selective integration displacement models for nonlinear shell analysis," in Nonlinear Finite Element Analysis of Plates and Shells, ed. by T.J.R. Hughes, et al, ASME, AMD-Vol. 48, 119-146 1981.

17. S.F. Pawsey "Discussion of paper by O.C. Zienkiewicz, R.L. Taylor and J.M. Too and S.F. Pawsey and R.L. Clough; Int. J. Num. Meth. Engrg., 4, 449-450, 1972.

18. R.D. Cook "More on reduced integration and isoparametric elements," Int. J. Num. Meth. Engrg., 5, 144-148, 1972.

19. N. Bicanic and E. Hinton, "Spurious modes in two-dimensional isoparametric elements," Int. J. Num. Meth. Engrg., 14, 1545-1557, 1979.

20. L.J. Hayes, "Practical stability test for finite elements with reduced integration," Int. J. Num. Meth. Engrg., 17, 1689-1695, 1981.

21. R.D. Cook and F. Zhao-Hua, "Control of spurious modes in the nine-node quadrilateral element," Int. J. Num. Meth. Engrg., 18, 1576-1580, 1982.

22. B.M. Irons and A. Razzaque, "Experience with the patch test for convergence of finite elements," in the Mathematical Foundations of the Finite Element Method with Applications to Partial Differential Equations, Ed. by A.K. Aziz, Academic Press, 589-602, 1972.

23. G. Strang, "Variational Crimes in the Finite Element Method," ibid, pp. 689-710.

24. T.J.R. Hughes, M. Cohen and M. Haroun, "Reduced and selective integration techniques in finite element analysis of plates," Nucl. Eng. Des. 46, 203-222 1978.

25. J. Robinson and H. Haggenmache, "ROLA, an accurate 4-node stress plate bending element," Int. J. Num. Meth. Eng., 14, No. 2, 296-306 1979.

List of Figure Captions

1. Nomeclature, local node numbers and quadrature points for 9-node Lagrange element.

2. Spurious singular mode $\underset{\sim}{h}$.

3. Problem description for example 1: square domain with prescribed temperature along boundary.

4. Temperature u along B-C for the three meshes for example 1 with $\varepsilon = 1.0$.

5. Temperature u along B-C for example 1 with medium mesh and $\varepsilon = 0.1$ and 1.0.

6. Problem description for example 2 and 3: circular domain with Neumann and Dirichlet boundaries.

7. Temperature u along the radius coincident with the x-axis for the medium mesh $\varepsilon = 10^{-5}$, 10^{-4}, and 1.0 for example 2.

8. Temperature u along the radius coincident with the x-axis for the three meshes for example 3 with $\varepsilon = 1.0$.

9. Temperature u along the radius coincident with the x-axis for example 3 with $\varepsilon = 0.1$ and 1.0.

10. Convergence rates for examples 1 (square) and 3 (circular) with 2 x 2 quadrature, $\varepsilon = 1.0$ and 3 x 3 quadrature.

11. Temperature distributions for example 4, showing the evolution of spurious oscillations with 2 x 2 quadrature in the absence of stabilization.

12. Displacement w along a radius, line B-C in Fig. 6, for a clamped, circular plate for two values of r_w.

13. Displacement w along a radius, line B-C in Fig. 6, for three meshes for the clamped, circular plate.

14. Convergence in L_2 norm, Eq. (7.1), for clamped square and circular plates with stabilization ($r_w = 0.1$, $r_\theta = 1.0$) and for selective reduced integration; the convergence rate when $\chi = \underset{\sim}{h}$ is also shown.

15. Displacements along a centerline for a uniformly loaded a x a square plate supported at the corners for various values of r_w.

16. Displacement of node adjacent to center for the corner supported plated and clamped plate for various values of r_w.

17. Displacement w along a radius, line B-C in Fig. 6, for a thick, circular plate with clamped supports for various values of r_w.

Table 1

Zero-Energy Modes At Biquadratic Plate Element U_2

		w	θ_x	θ_y	Name
Rigid body modes	1	$\underset{\sim}{s}^T$	$\underset{\sim}{0}^T$	$\underset{\sim}{0}^T$	Translation
	2	$-\underset{\sim}{x}^T$	$\underset{\sim}{0}^T$	$\underset{\sim}{s}^T$	y - rotation
	3	$\underset{\sim}{y}^T$	$\underset{\sim}{s}^T$	$\underset{\sim}{0}^T$	x - rotation
Kinematic modes	1	$\underset{\sim}{h}^T$	$\underset{\sim}{0}^T$	$\underset{\sim}{0}^T$	w - spurious
	2	$\underset{\sim}{0}^T$	$\underset{\sim}{s}^T + 3\underset{\sim}{h}^T$	$\underset{\sim}{0}^T$	θ_x - spurious
	3	$\underset{\sim}{0}^T$	$\underset{\sim}{0}^T$	$\underset{\sim}{s}^T + 3\underset{\sim}{h}^T$	θ_y - spurious
	4*	$\underset{\sim}{0}^T$	$(\underset{\sim}{s}^T + 3\underset{\sim}{h}^T)\hat{Y}$	$(\underset{\sim}{s}^T + 3\underset{\sim}{h}^T)\hat{X}$	twist

where $\underset{\sim}{x} = \hat{\underset{\sim}{X}}\,\underset{\sim}{s}$, $\underset{\sim}{y} = \hat{\underset{\sim}{Y}}\,\underset{\sim}{s}$, $\hat{X}_{ij} = x_i\delta_{ij}$ and $\hat{Y}_{ij} = y_i\,\delta_{ij}$
and there is no sum on i.

* At the present time, this mode is valid for rectangular shape element only.

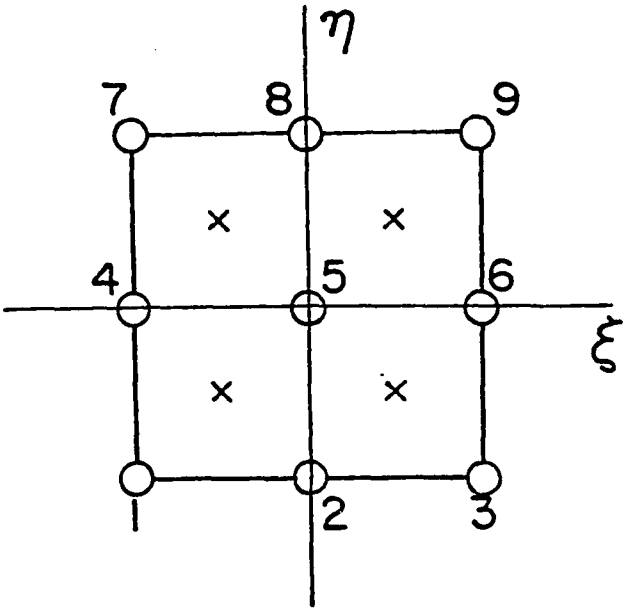

Reference plane

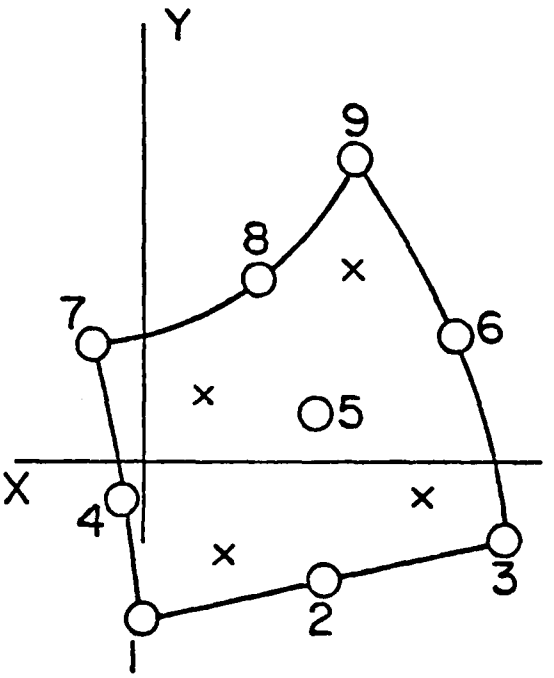

Physical plane

○ node

× quadrature point

(1)

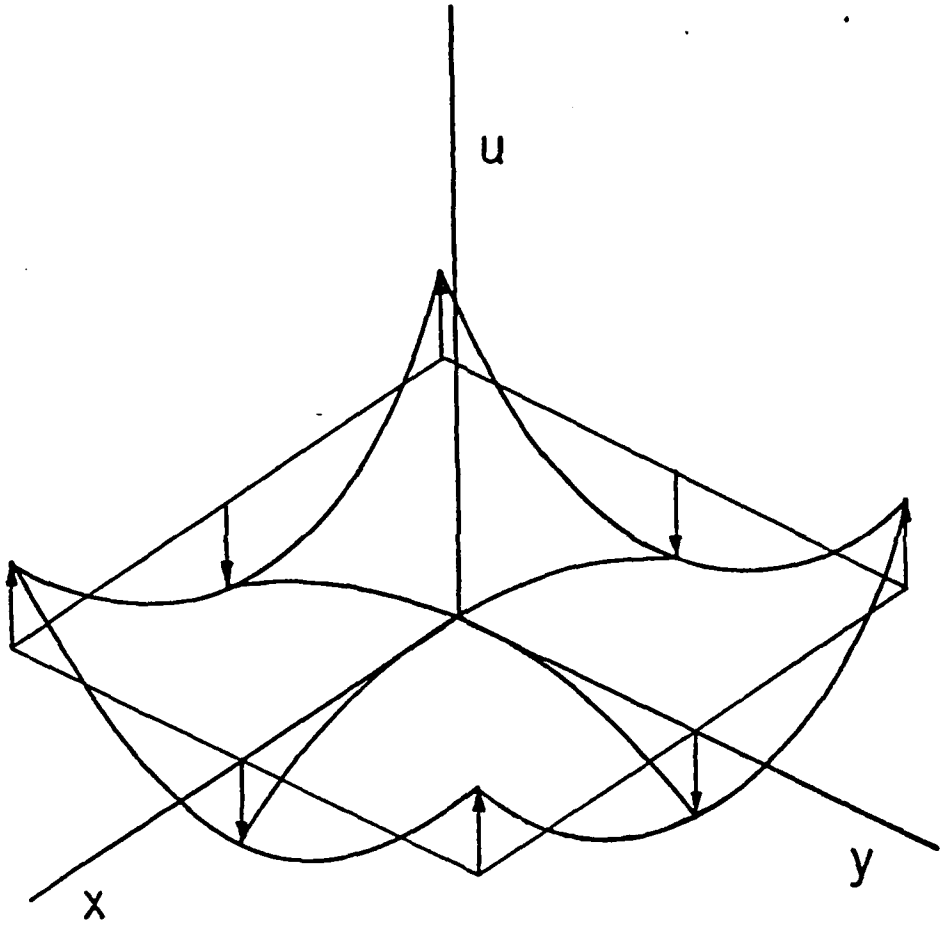

(2)

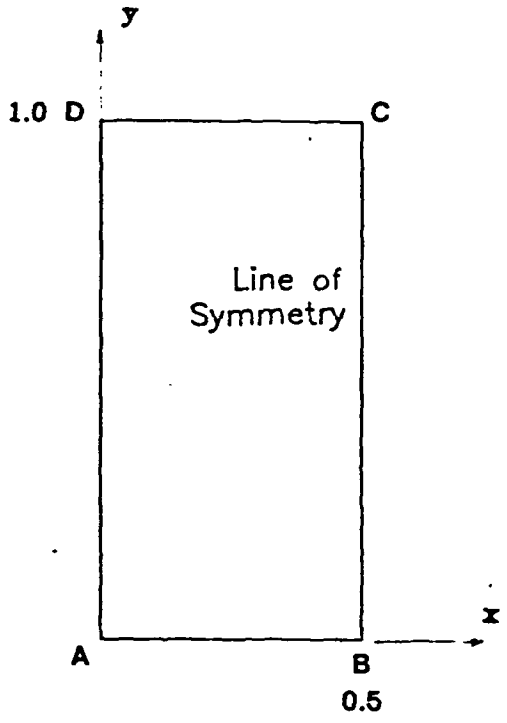

$s = 0$

$\alpha_{ij} = 0.005\ \delta_{ij}$

Boundary cond.

$u(0,y) = 0$ $\quad 0<y<1$

$u(x,1) = 0$ $\quad 0<x<0.5$

$u(x,0) = \sin \pi x$ $\quad 0<x<0.5$

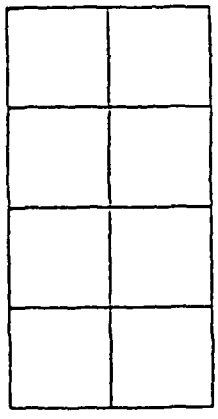

Mesh A

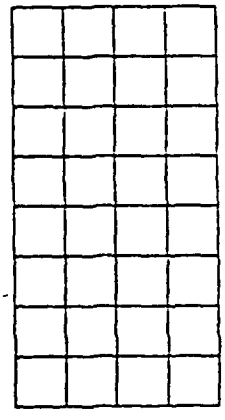

Mesh B

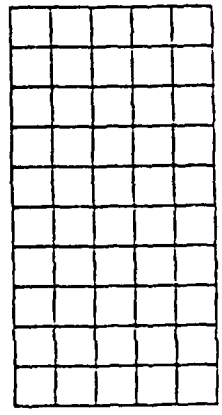

Mesh C

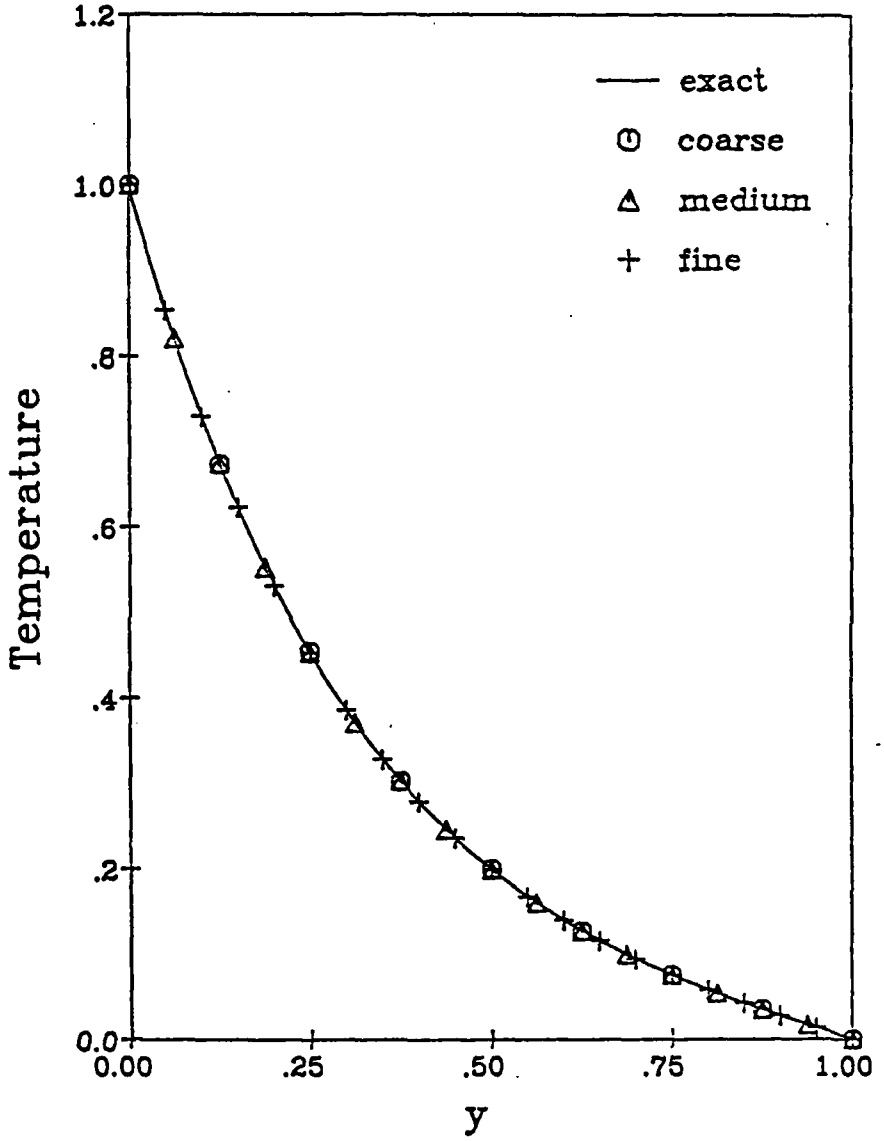
1.2
1.0
.8
.6
.4
.2
0.0
Temperature
0.00
.25
.50
.75
1.00
y
exact
coarse
medium
fine

④

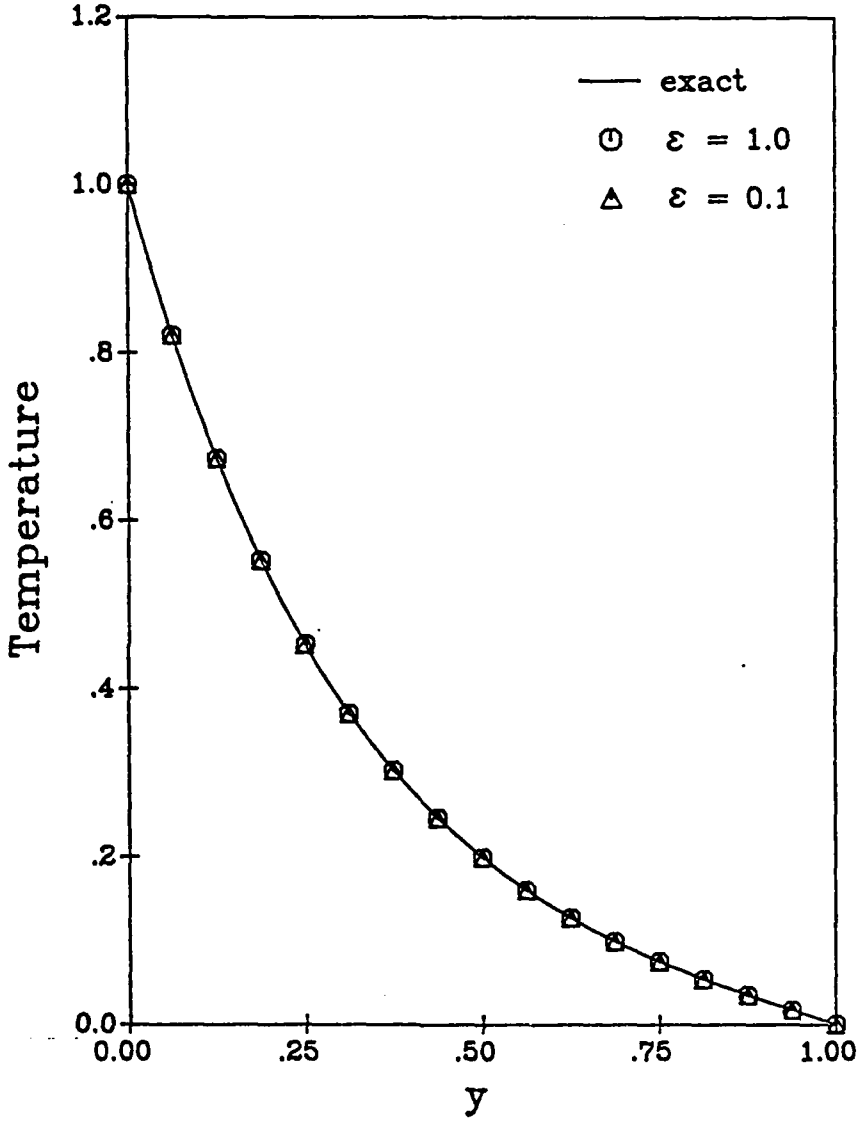

(5)

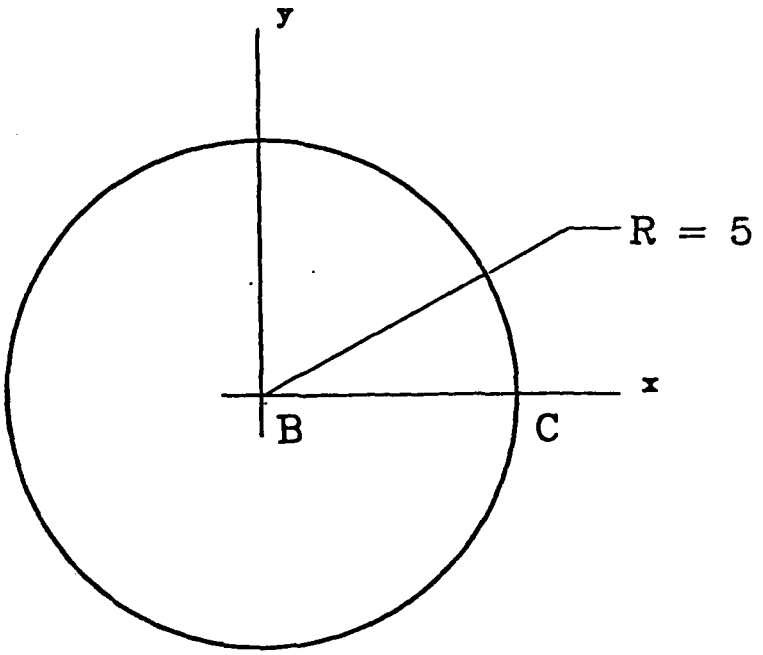

s = 0

$\alpha_{ij} = 0.04\ \delta_{ij}$

Boundary cond.

example 2

$u_{,r}(r=5) = 62.5$

$u(r=0) = 0$

example 3

$u(r=5) = 0$

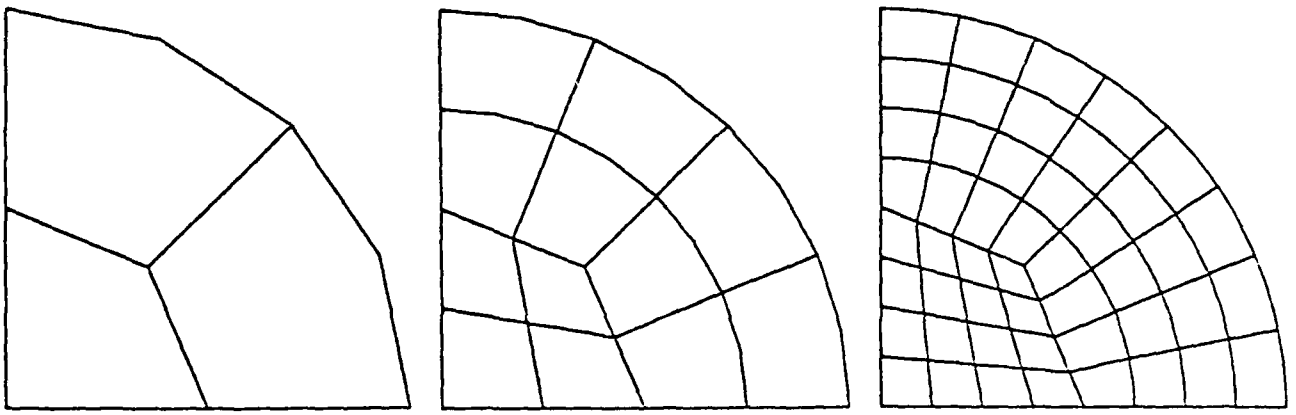

Mesh A Mesh B Mesh C

(6)

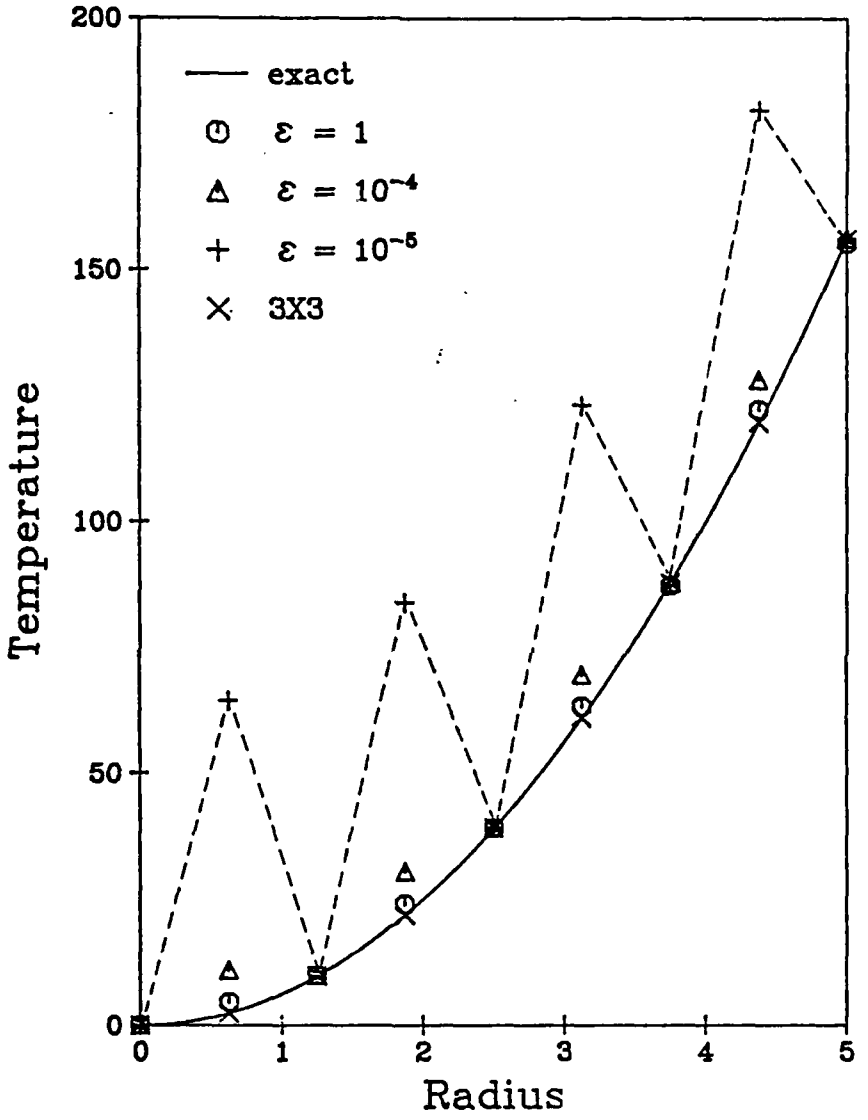
200
150
100
50
0
Temperature
exact
ε = 1
ε = 10⁻⁴
ε = 10⁻⁵
3X3
0
1
2
3
4
5
Radius

(7)

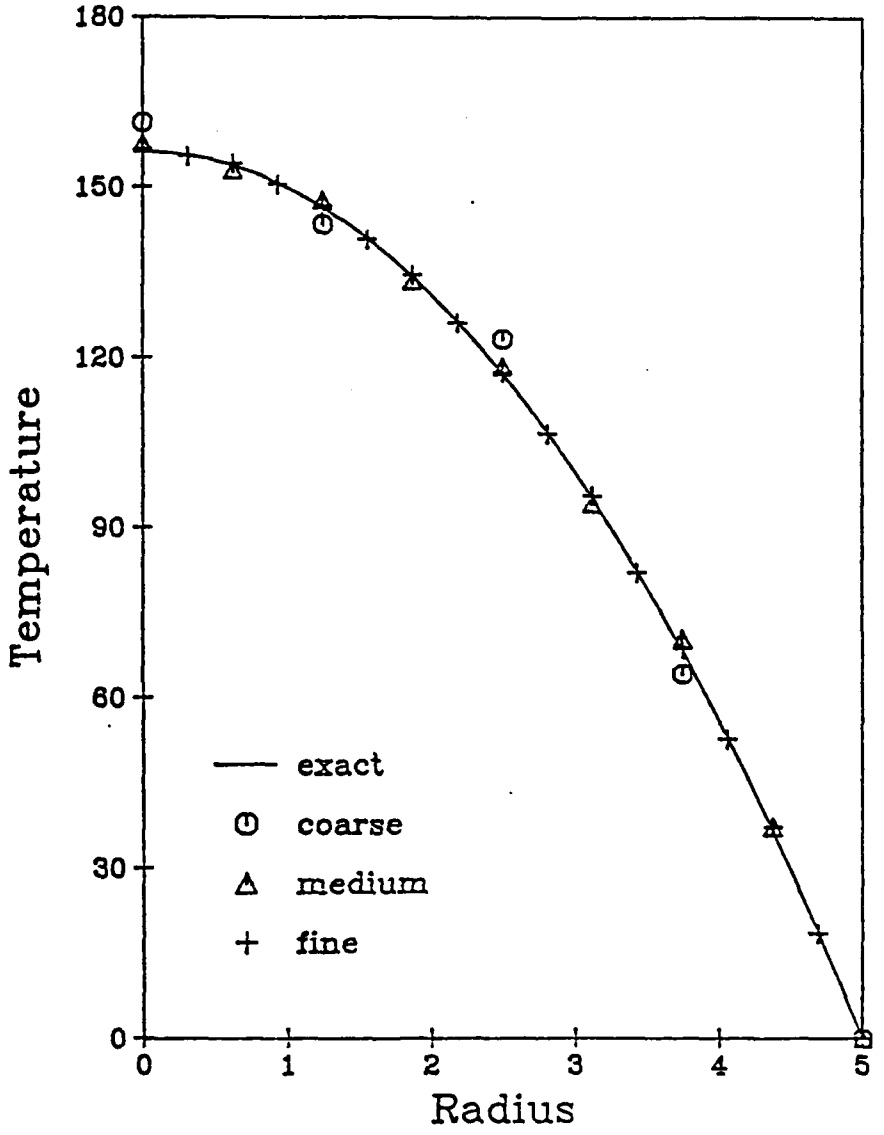
180
150
120
90
60
30
0
Temperature
0
1
2
3
4
5
Radius
exact
coarse
medium
fine

(e)

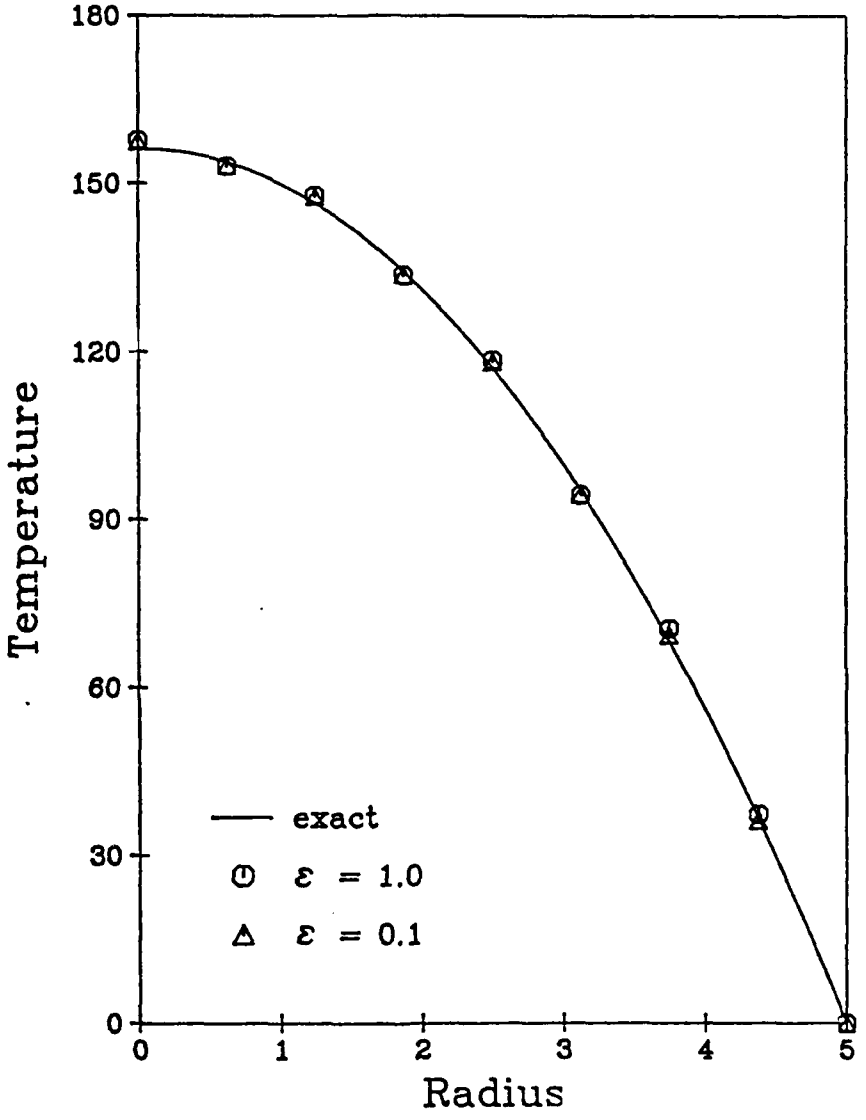
180
150
120
90
60
30
0
Temperature
0
1
2
3
4
5
Radius
exact
ε = 1.0
ε = 0.1

⑨

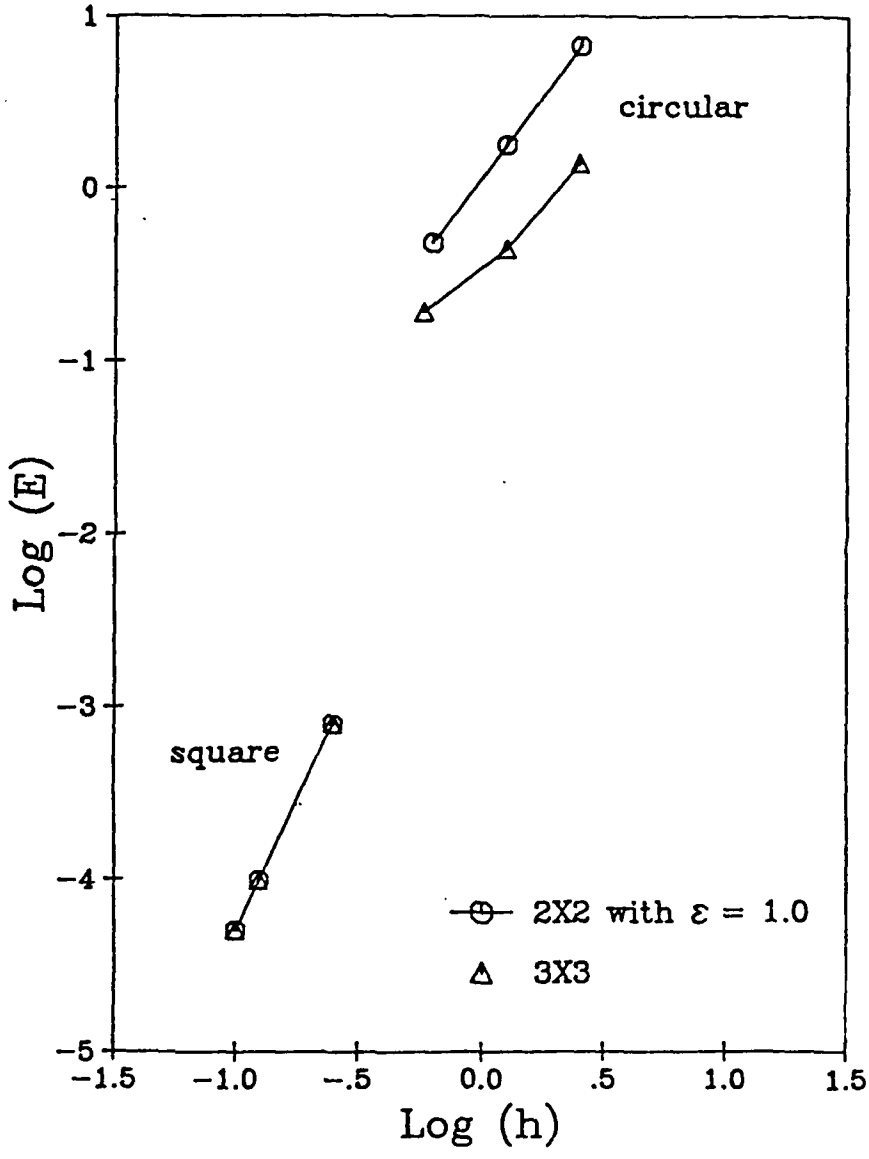
1
0
−1
−2
−3
−4
−5
Log (E)
−1.5
−1.0
−.5
0.0
.5
1.0
1.5
Log (h)
circular
square
2X2 with ε = 1.0
3X3

(10)

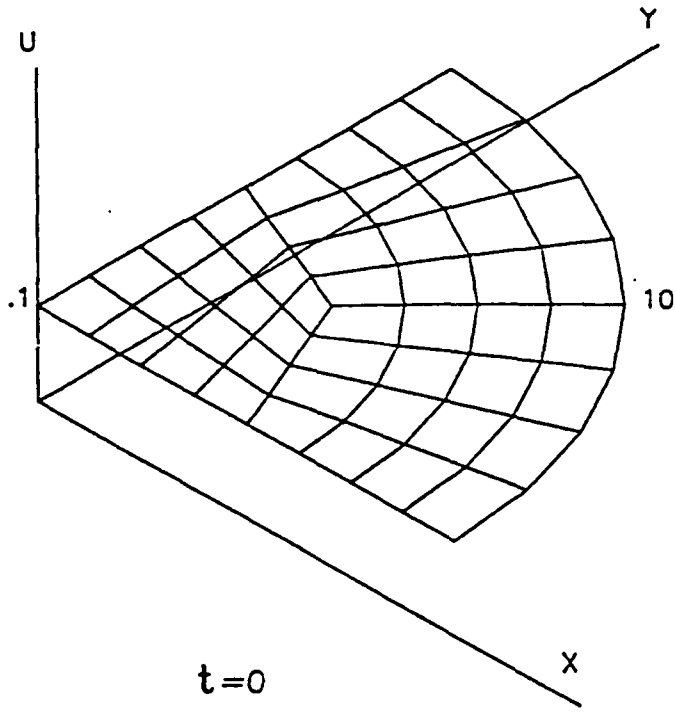

t=0

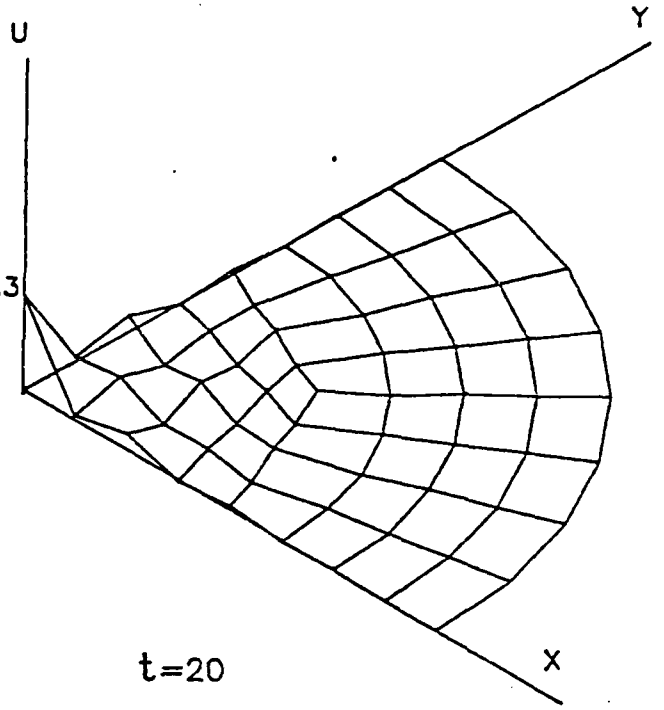

t=20

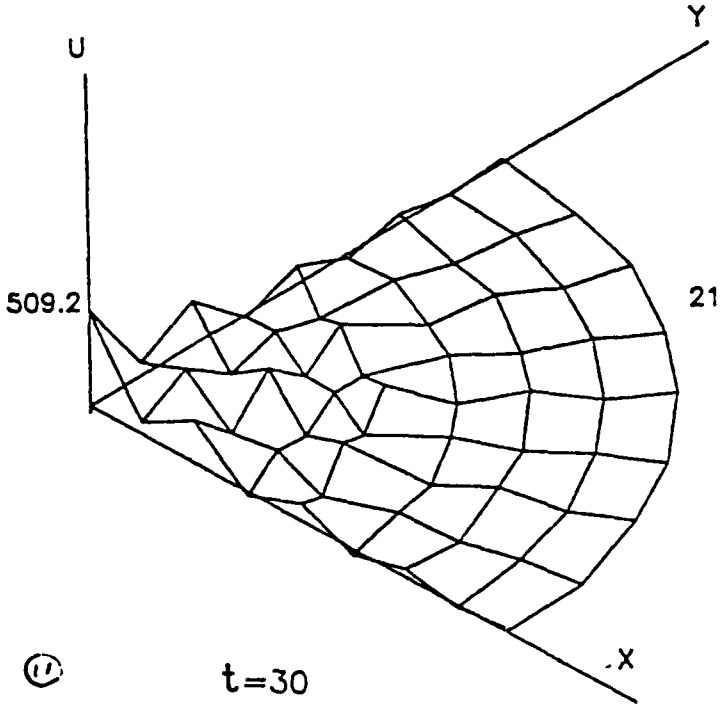

t=30

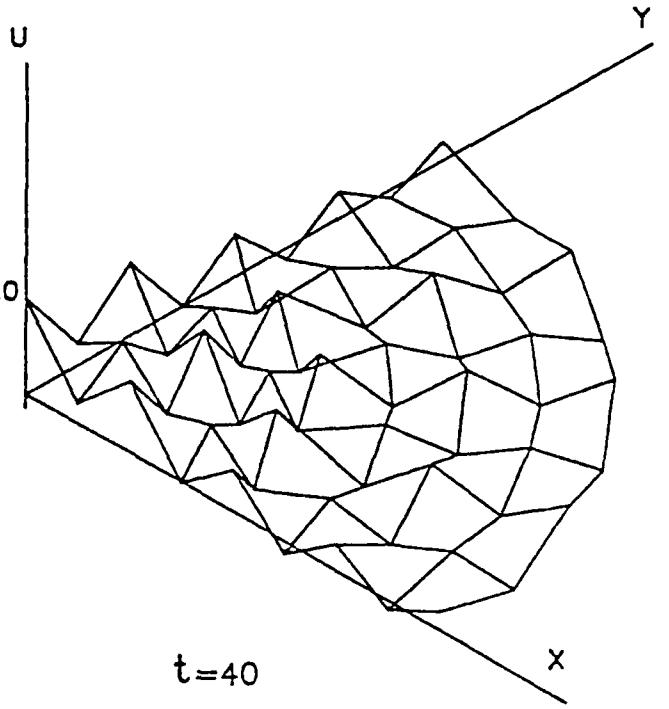

t=40

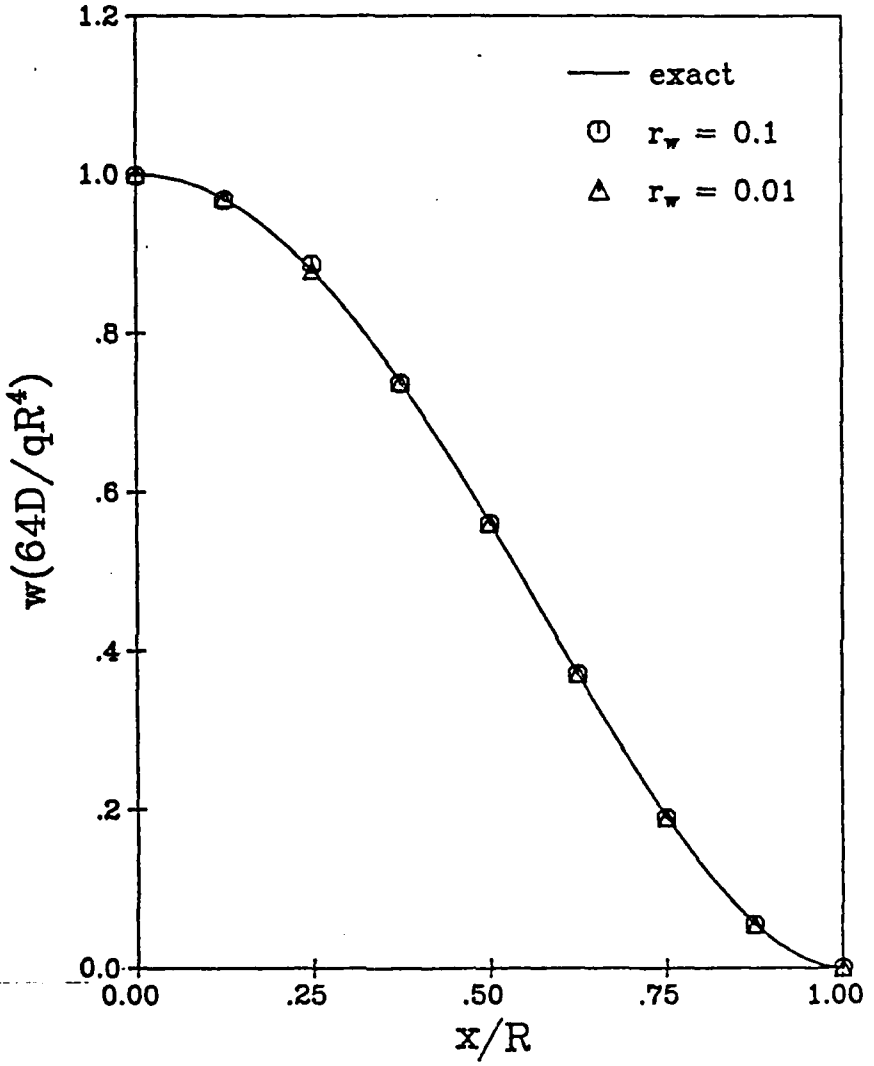

(12)

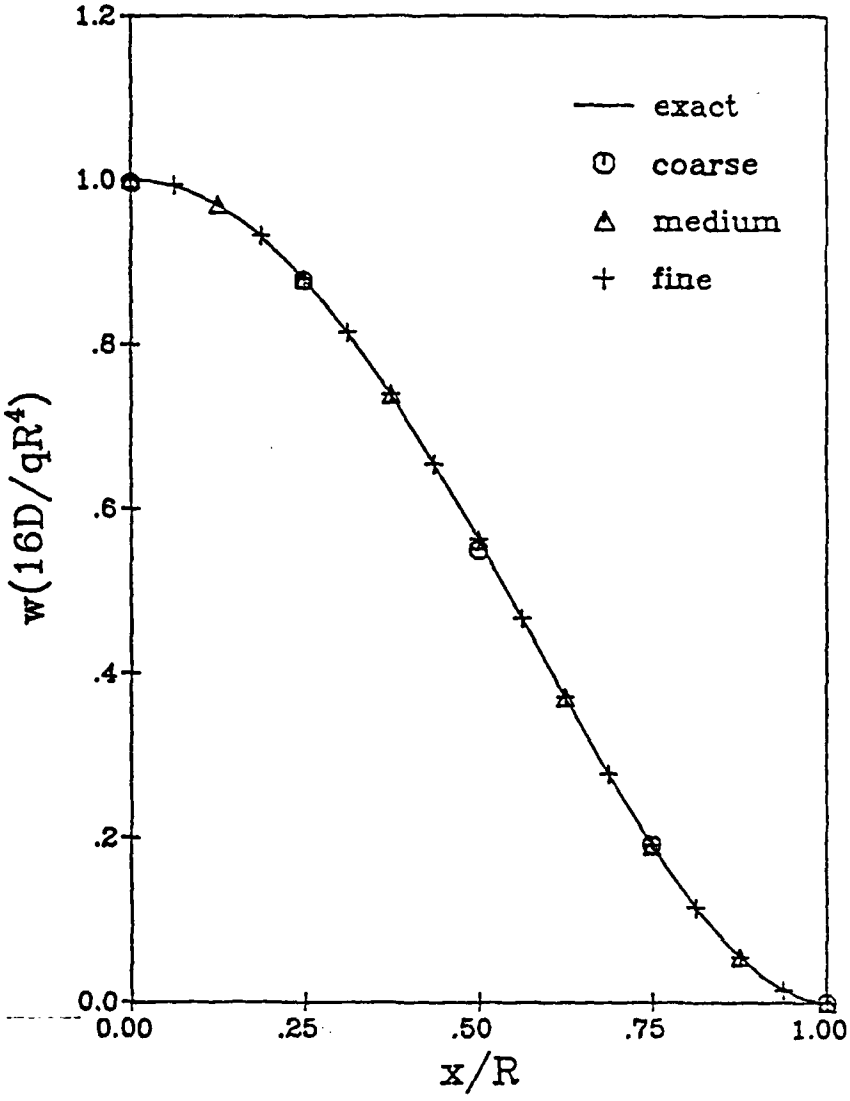
1.2
1.0
.8
.6
.4
.2
0.0
0.00
.25
.50
.75
1.00
w(16D/qR⁴)
x/R
exact
coarse
medium
fine

(13)

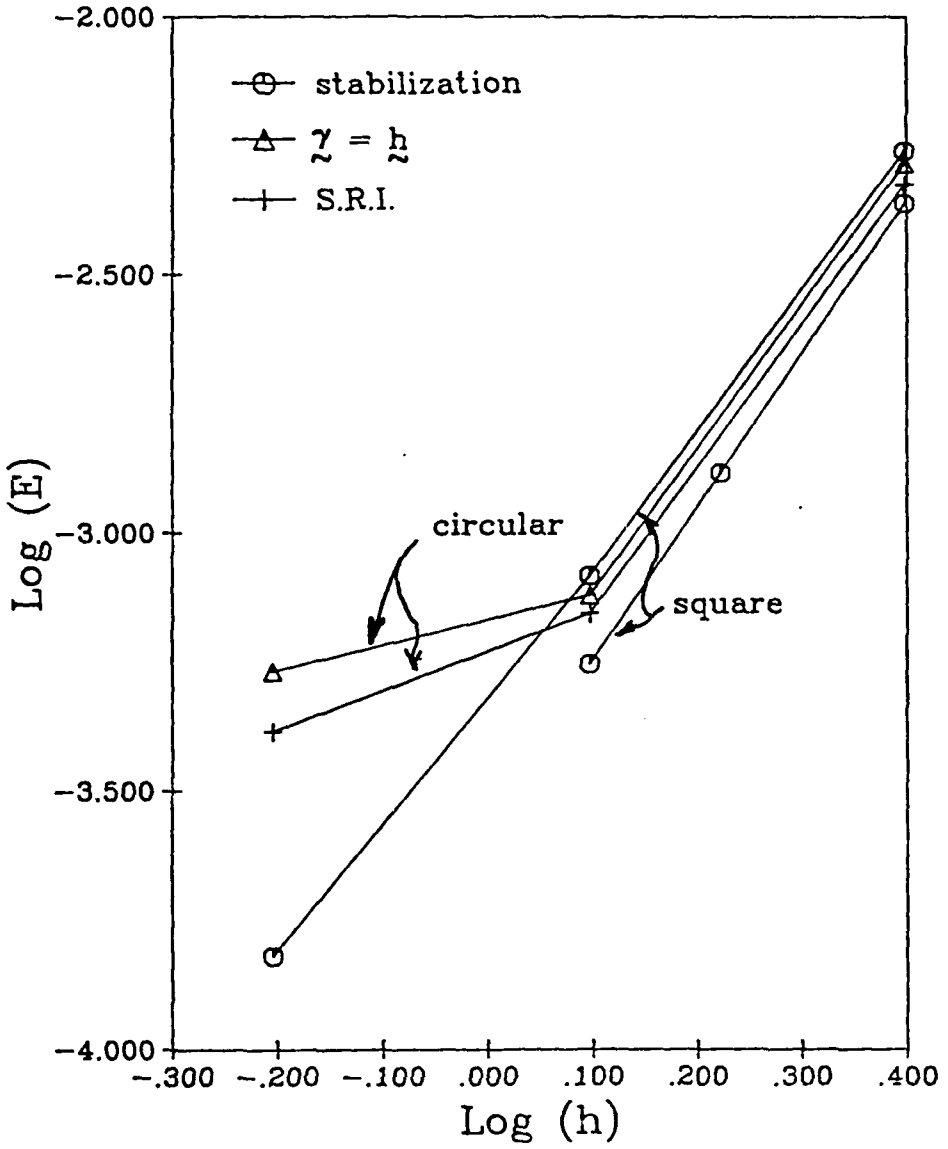
stabilization
γ = h
S.R.I.
circular
square
Log (E)
Log (h)
-2.000
-2.500
-3.000
-3.500
-4.000
-.300
-.200
-.100
.000
.100
.200
.300
.400

(14)

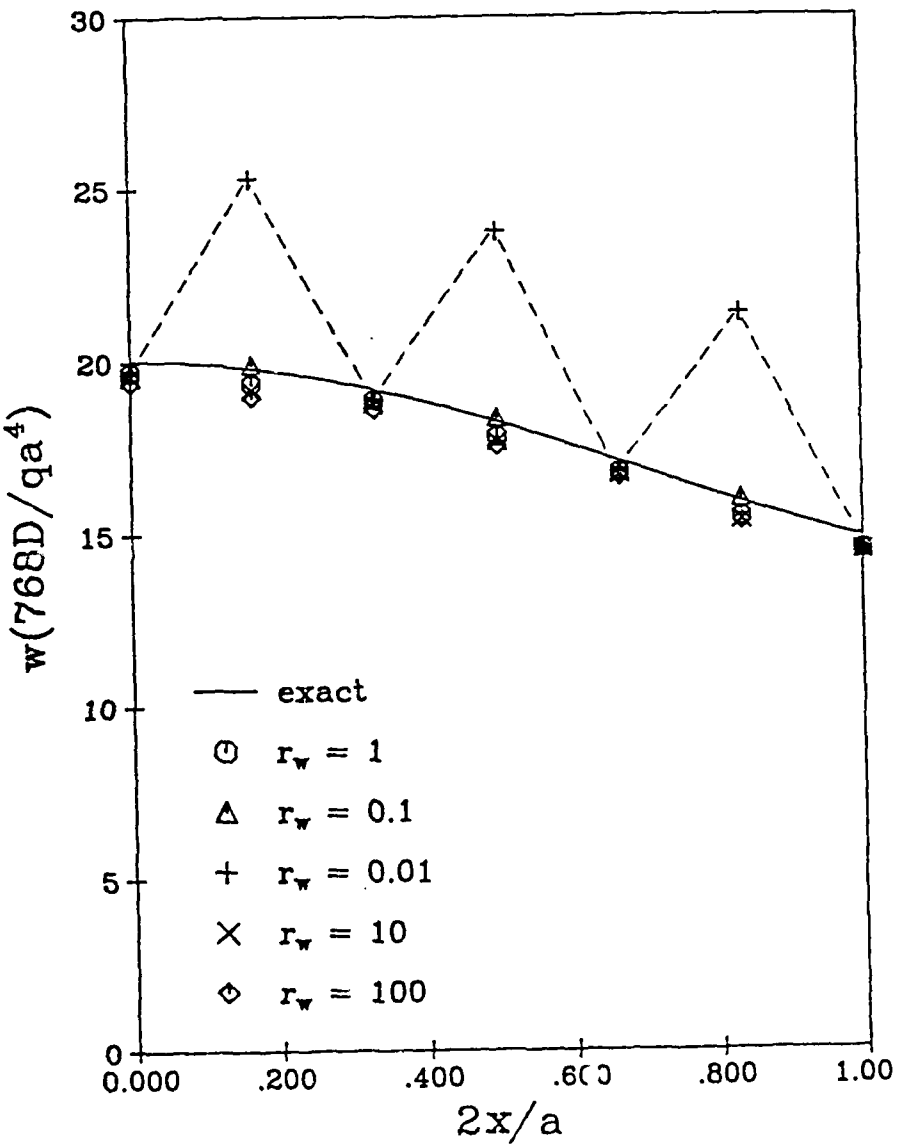
30
25
20
15
10
5
0
0.000
.200
.400
.600
.800
1.00
2x/a
w(768D/qa⁴)
exact
r_w = 1
r_w = 0.1
r_w = 0.01
r_w = 10
r_w = 100

(15)

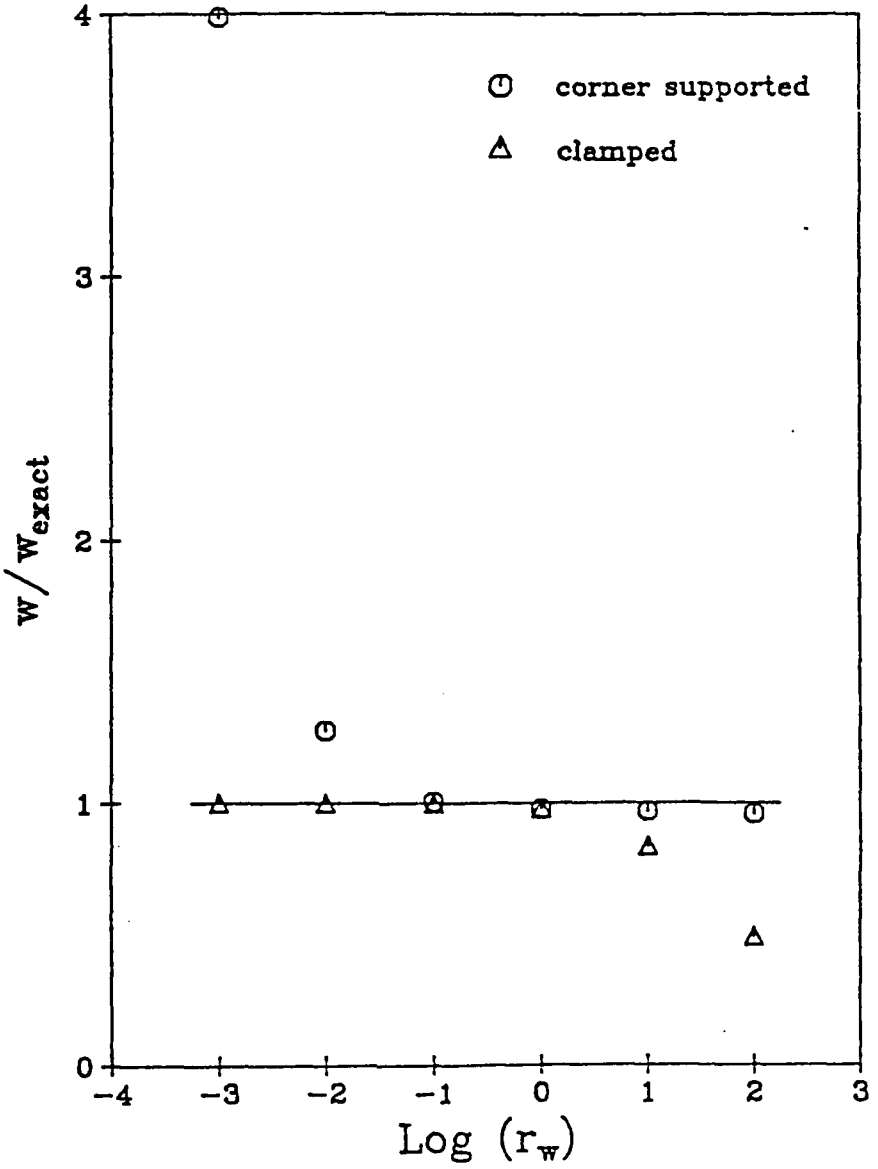

(16)

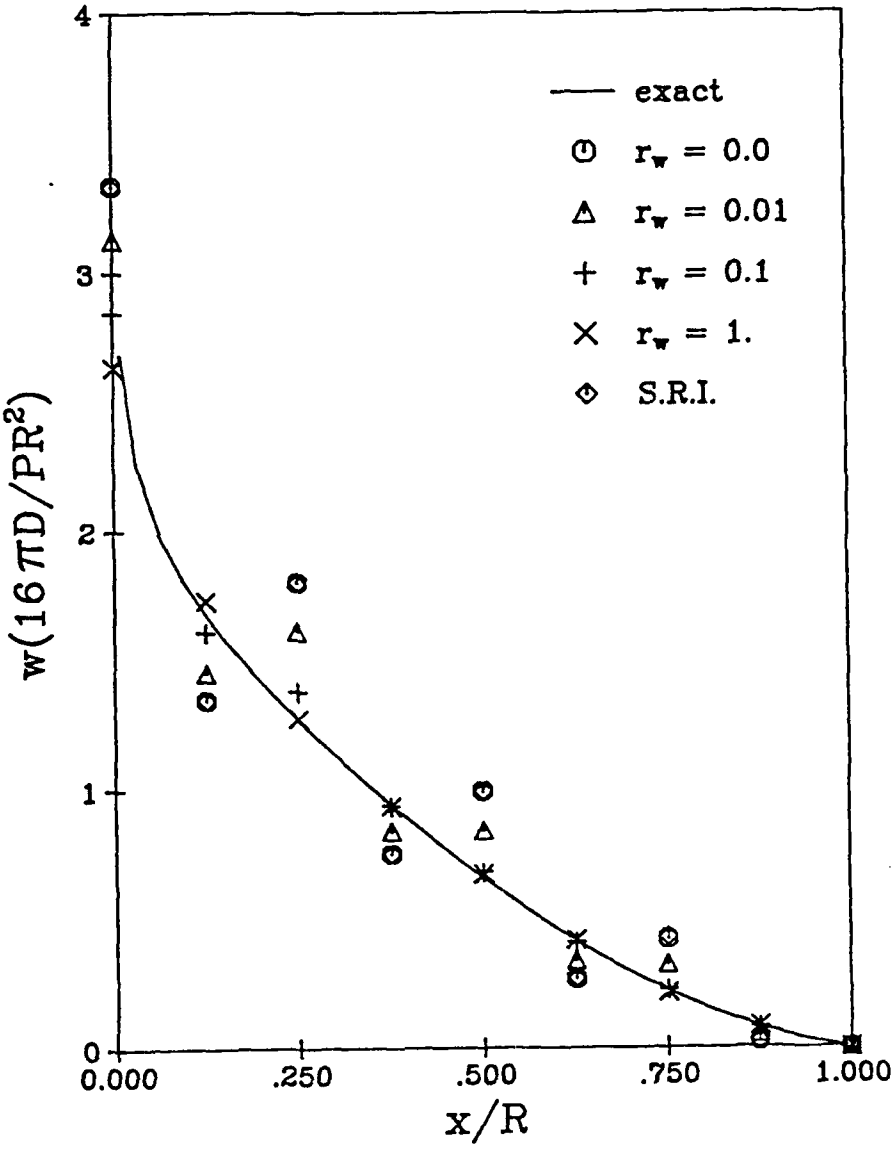
exact
r_w = 0.0
r_w = 0.01
r_w = 0.1
r_w = 1.
S.R.I.
$w(16\pi D/PR^2)$
x/R
0
1
2
3
4
0.000
.250
.500
.750
1.000

(17)

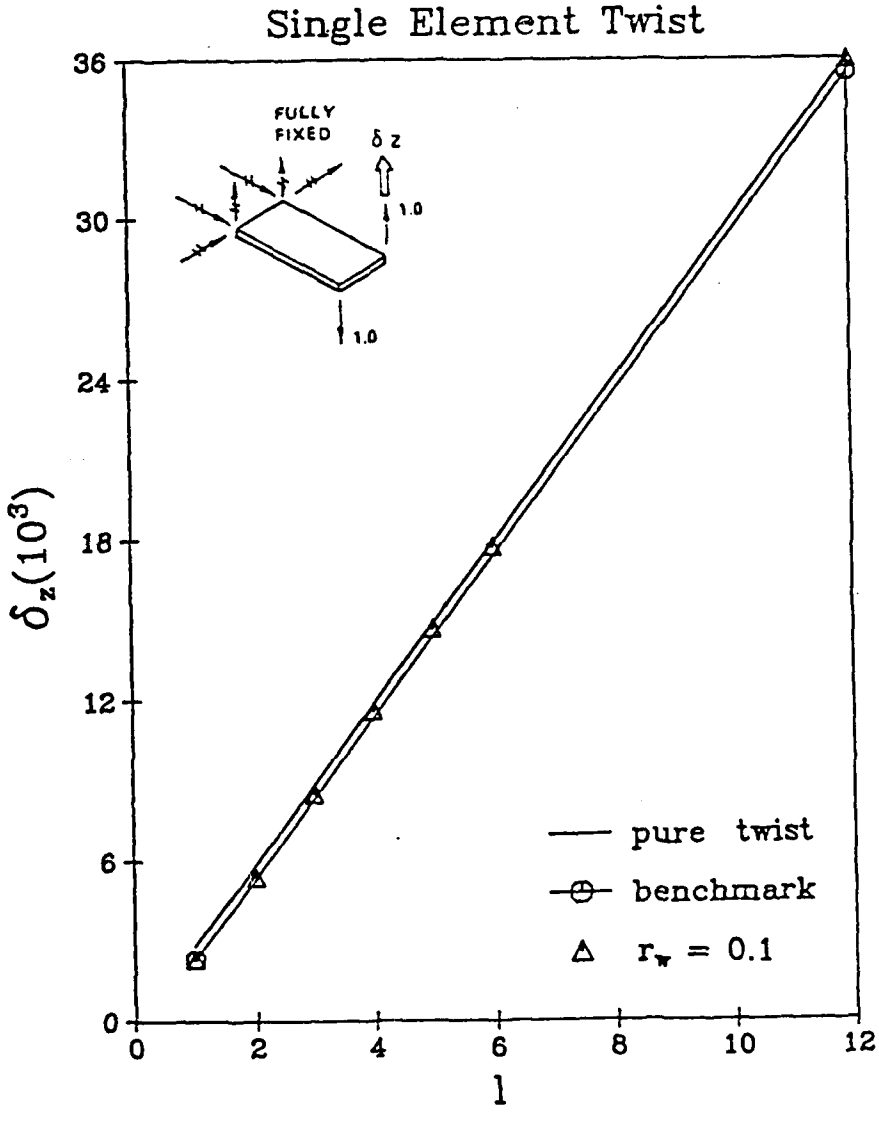
Single Element Twist
FULLY FIXED
δ z
1.0
1.0
36
30
24
18
12
6
0
$\delta_z(10^3)$
0
2
4
6
8
10
12
l
pure twist
benchmark
$r_w = 0.1$

(18)

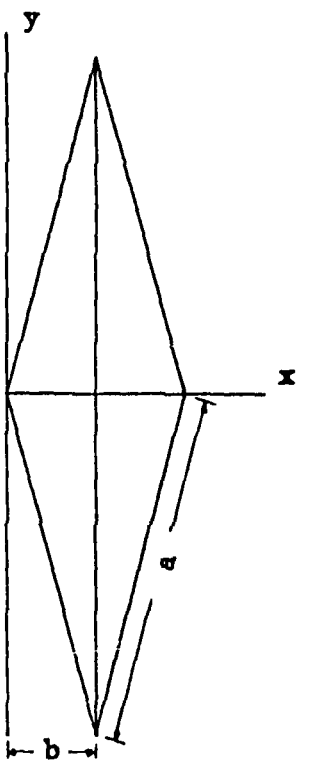

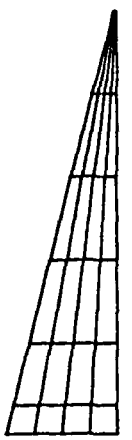

Mesh A

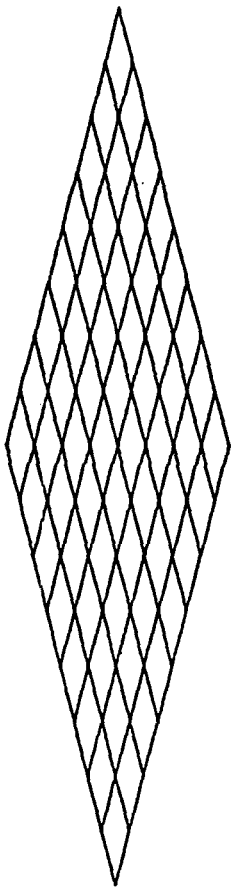

Mesh B

simple supported edges
uniform load q
a = 100 in h = 0.1 in
b = 25.9 in ν = 0.3

(19)

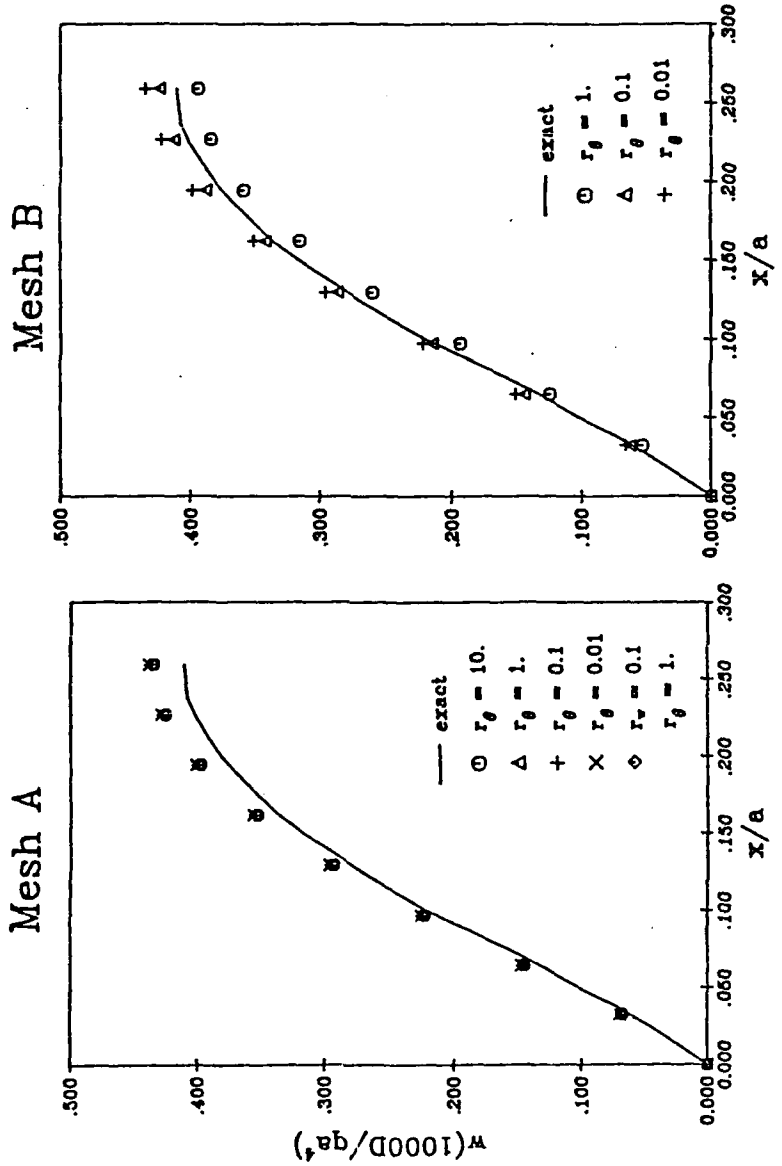
Mesh A
Mesh B
w(1000D/qa⁴)
x/a
exact
r_θ = 10.
r_θ = 1.
r_θ = 0.1
r_θ = 0.01
r_r = 0.1
r_θ = 1.
0.000
.050
.100
.150
.200
.250
.300
.100
.200
.300
.400
.500

(20)

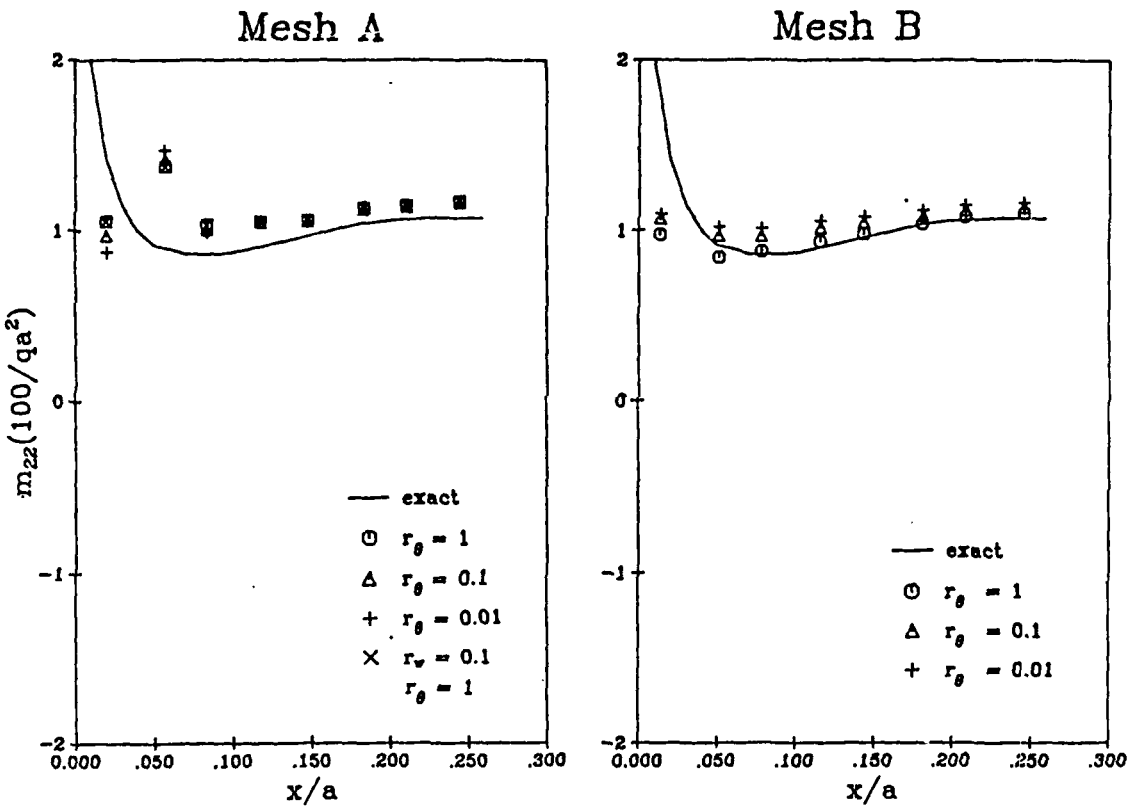
Mesh A
Mesh B
$m_{22}(100/qa^2)$
x/a
exact
$r_\theta = 1$
$r_\theta = 0.1$
$r_\theta = 0.01$
$r_w = 0.1$
$r_\theta = 1$
2
1
0
-1
-2
0.000
.050
.100
.150
.200
.250
.300

(21)

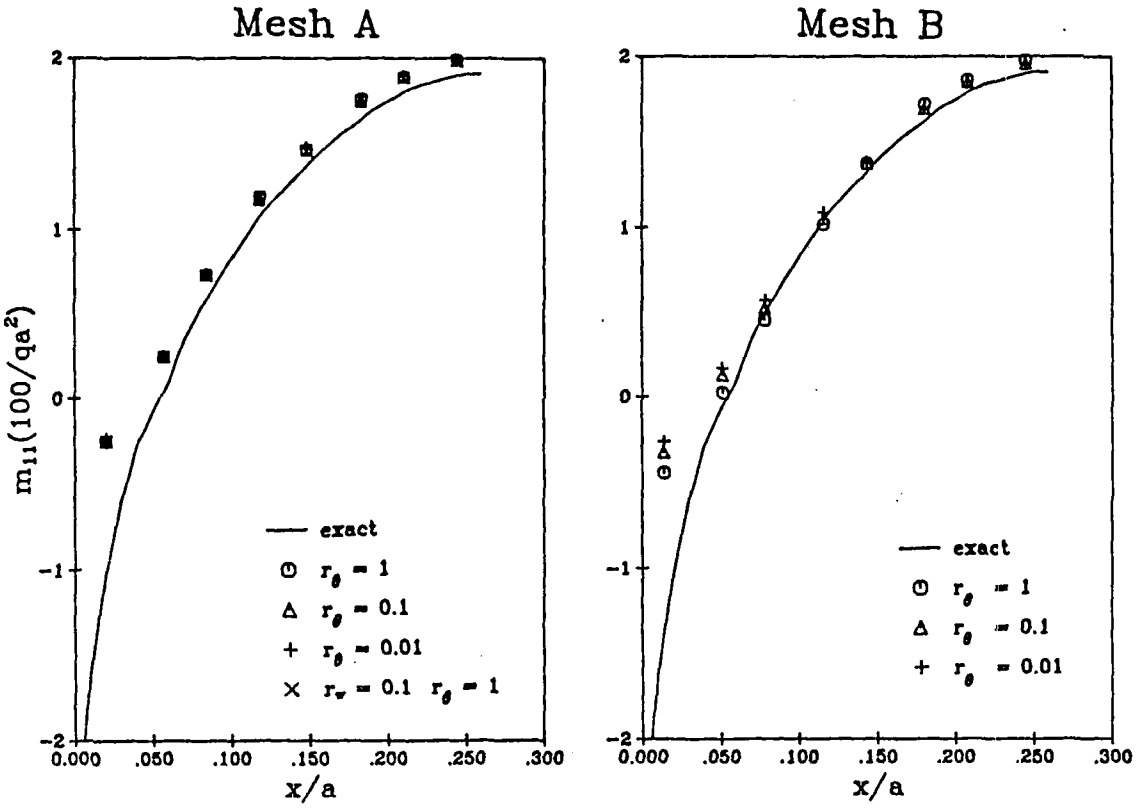
Mesh A
Mesh B
$m_{11}(100/qa^2)$
x/a
exact
r_θ = 1
r_θ = 0.1
r_θ = 0.01
r_w = 0.1 r_θ = 1
0.000
.050
.100
.150
.200
.250
.300
2
1
0
-1
-2

22

END

12-86

DTIC